Groundwater for Sustainable Development 24 (2024) 101063

Contents lists available at ScienceDirect

Groundwater for Sustainable Development

journal homepage: www.elsevier.com/locate/gsd

Research paper

Application of autochthonous extremophilic *Bacillus xiamenensis* in remediation of groundwater- A sorption-based metal cleaning approach

Kasturi Charan [a], Jajati Mandal [b,*], Pradip Bhattacharyya [a]

[a] Agricultural and Ecological Research Unit, Indian Statistical Institute, Giridih, Jharkhand, 815301, India
[b] School of Science, Engineering & Environment, University of Salford, Manchester, M5 4WT, UK

HIGHLIGHTS

- Biosorption efficiency of *Bacillus xiamenensis* ISIGRM16 followed the order Cd^{2+}>Ni^{2+}>Cr^{6+}.
- Best fit adsorption isotherms: Freundlich (Cd^{2+}), Langmuir (Ni^{2+}, Cr^{6+}).
- Relative adsorption capacity (multi-component system): 92.57% (Ni^{2+}), 90.66% (Cd^{2+}) and 82.46% (Cr^{6+}).
- Effective metal clean-up potential up to 3rd cycle making it a sustainable product.

GRAPHICAL ABSTRACT

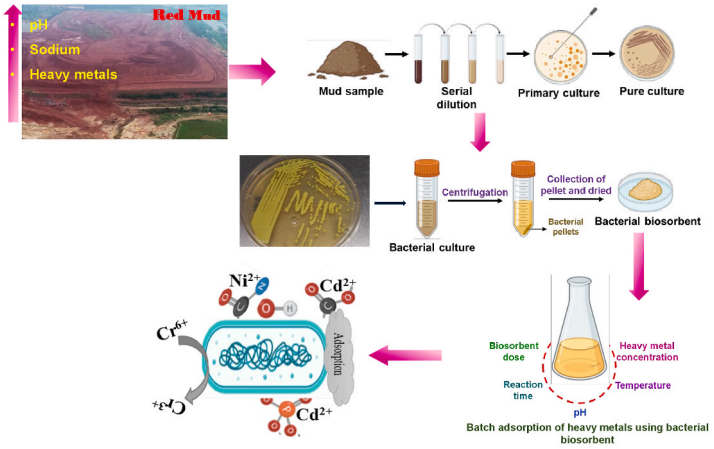

ARTICLE INFO

Keywords:
Adsorption models
Biosorption
Heavy metals
Polyextremophilic
Relative adsorption capacity
Thermodynamics

ABSTRACT

Surface water and groundwater used for drinking and agricultural purposes are contaminated due to anthropogenic and geogenic activities. Escalated metal concentrations, xenobiotic pollutants, competitive ions, and reusability issues are main hindrances towards decontamination of water. Moreover, the expensive purification technology brings obstacles to the underdeveloped community from availing clean water. In this context, the present work offers a sustainable cost-effective approach by providing an effective and sustainable sorption-based purification method by novel polyextremophilic bacteria *Bacillus xiamenensis* ISIGRM16 isolated from metal-rich industrial waste, red mud. Batch adsorption study revealed that the bacterium can remove Cd^{2+}(>99%), Ni^{2+}(>85%), and Cr^{6+}(>40%) from aqueous solution. The optimum parametric conditions for the removal of Cd^{2+} and Ni^{2+} were observed at a temperature of 30 °C and a pH of 6, while for Cr^{6+} removal, the optimal conditions were a temperature of 45 °C and a pH of 2. The adsorption process of Cd^{2+} was best explained by Freundlich isotherm ($R^2 \geq 0.95$), revealing multilayer adsorption. Ni^{2+} and Cr^{6+} followed the Langmuir isotherm, indicated adsorption onto the monolayer surface. The interaction mechanism was determined to be following 2nd order kinetics, with both exothermic (Cd^{2+}, Ni^{2+}) and endothermic (Cr^{6+}) characteristics. The

* Corresponding author.
E-mail address: j.mandal2@salford.ac.uk (J. Mandal).

https://doi.org/10.1016/j.gsd.2023.101063
Received 9 October 2023; Received in revised form 28 November 2023; Accepted 3 December 2023
Available online 7 December 2023

maximum adsorption capacities were found to be 31.42, 29.30, and 15.21 mg g^{-1} for Cd^{2+}, Ni^{2+}, and Cr^{6+} respectively. In the ternary system, the adsorption capacity followed the order $Ni^{2+} > Cd^{2+} > Cr^{6+}$, as confirmed by both their relative adsorption capacity and from analysis visual MINTEQ. Microscopic and spectroscopic analyses revealed, altered cell morphology, metal deposition on the bacterial cell surface, and the involvement of hydroxyl, carboxyl, and amide groups in the elimination of Cd^{2+}, Ni^{2+}, and Cr^{6+}. Further the sequential adsorption-desorption study confirmed a significantly preserved removal efficacy ($p < 0.05$), indicating the advantageous use of the bacterium as a biosorbent.

1. Introduction

Water is the source of life on Earth and one-third of the world's population relies exclusively on groundwater for drinking. Approximately 65% of groundwater is allocated for human consumption, 20% for irrigation, and 15% for industrial activity (Adimalla and Sudarshan, 2018). Access to clean water is fundamental for maintaining a healthy life. However, challenges persist for half of the world population especially in developing countries due to inadequate access to clean water and improper sanitation (United Nations Development Programme, 2006). Different kinds of chemical contamination of both surface and groundwater without proper remediation disrupt the harmonic relation between nature and human society.

Heavy metal (HM) encompasses a group of elements containing numerous toxic metals and metalloids with high molecular weight and atomic density (Dhaliwal et al., 2019). HM pollution originating from diverse point and non-point sources like domestic sewage, industrial effluent, and geogenic factors has been a persistent and century-old concern. The non-degradability and prolonged persistence of HMs like cadmium (Cd), nickel (Ni), chromium (Cr), lead (Pb), copper (Cu), arsenic (As), cobalt (Co), mercury (Hg) lead to several epidemic glitches in human civilization. Millions of rural households across the globe are vulnerable to contaminated water. There are reports of health hazards like memory loss, gastrointestinal problems, bronchial damage, cancer, renal failure, mental retardation, and chronic diseases. These issues pose epidemiological challenges, particularly among the people who are poor and lack access to expensive and not easily available technologies. Among the affected, women and children are vulnerable as they are more exposed to such contamination, resulting in a growing burden of health-related expenses on rural poor subjected to industrial effluents. Overall, the entire ecosystem experiences the intimidating effects of HM bioaccumulation and subsequent biomagnification via the food chain (Mahanty et al., 2020; Majhi et al., 2023). Cd, Ni, and Cr are the three predominant HMs found in polluted water across the country and the globe (Karunanidhi et al., 2022). They are mainly discharged through effluents from different industries like electroplating, leather tanning, wood preservation, pulp processing, steel manufacturing, etc. Their long-term accumulation in the soil further leaches over time, contaminating both surface and groundwater (Congeevaram et al., 2007; Dong et al., 2019). The World Health Organisation (WHO) established 0.01, 0.05, and 0.05 mg L^{-1} as the permitted limits for Cd, Ni, and Cr in potable water (Kumar et al., 2018). Furthermore, the International Agency for Research on Cancer refers to Cd^{2+} and Cr^{6+} as potent carcinogens (Jaishankar et al., 2014; J. Chakraborty et al., 2018). Likewise, Ni-containing compounds possess carcinogenic, mutagenic, and teratogenic properties (Gupta et al., 2019). The lack of remediation of contaminated groundwater/surface water poses a critical challenge in providing safe water for domestic and agricultural uses. Hence, recycling and remediation become a topmost priority. The remediation process of the present study, can effectively regenerate soil and water health, protect the environment, and be applicable in poor socio-economic conditions.

To date, numerous technologies (soil washing, ion exchange, chemical precipitation, gradient electrophoresis, membrane filtration, and electrocoagulation) have been employed for metal removal. However, their high cost, secondary pollutant generation, high energy requirement hinders their effectiveness (V. Chakraborty et al., 2018; Gupta et al., 2019; Majhi et al., 2022, 2023). Therefore environment-friendly, cost-effective remedial strategies using biological components like bacteria, fungus, plant residue, or agricultural waste could serve as commendable alternatives for absorbing and adsorbing or degrading xenobiotic toxicants (Giovanella et al., 2020). Bacterial bioremediation of metal is accomplished through different external and internal physiological processes (Manasi et al., 2014). Bacteria in metal-rich environments employ strategies like adsorption, intracellular accumulation according to metabolic requirements, precipitation, and oxidation-reduction to mitigate metal toxicity (Manasi et al., 2014; Majhi et al., 2022). Surface adsorption is a physicochemical process that involves binding metal ions with specific biomass through complexation, ion exchange, or electrostatic interaction while the intracellular mechanism is more complex and encompasses sequestration, chelation, efflux pump, etc. (Chatterjee et al., 2022; Majhi et al., 2023). Researchers highlight the benefits, availability, economic importance, and good performance at low concentrations, emphasizing the biosorption or biodegradation of metallic pollutants. However, the enhanced surface area-to-volume ratio and sorbent polarity significantly influence the performance of biosorption for any biosorbent (Chatterjee et al., 2022).

Red mud (RM), a waste product from the aluminium industry, poses environmental concerns due to its elevated sodium (Na^{+})-induced alkalinity and high occurrence of toxic metals (Cu, Cd, Pb, Ni, Cr, As, etc.) (Di Carlo et al., 2019, 2020). Such an extreme environment often serves as a reservoir of extremophilic organisms that possess phenotypic or genotypic plasticity adapting to long-term persistence in such unfavourable environments (Giovanella et al., 2020). Although many studies previously investigated the toxicity of metallic pollutants of RM on plants (Di Carlo et al., 2019) and microbial diversity of alkaline RM (Krishna et al., 2014), the use of RM-inhabiting bacteria in bioremediation purposes remains unexplored.

This study aims to explore the competence of indigenous bacteria in RM as a biosorbent for removing three toxic metals (Cd^{2+}, Cr^{6+}, Ni^{2+}) under specific conditions to encourage sustainable bioremediation of metallic pollutants through a cost-effective and straightforward technology. To the best of our knowledge, this study represents the first attempt to isolate polyextremophilic indigenous species from RM that exhibit multi-metal biosorption potential. The objectives were to isolate extremophilic bacteria and comprehend their role in reducing metal contamination. The biosorption mechanism was further assessed using an adsorption model and thermodynamic analysis. Further, we examined the biosorption potential of the bacteria in both mono-component and multi-component systems along with the effect of interfering ions on the removal behaviour.

2. Material and methods

2.1. Reagents

Standard stock solution (1000 mg L^{-1}) for Cd, Ni and Cr was obtained from Merck, Germany. Emsure grade ethanol was acquired from Merck, Millipore. Other chemicals like Glucose, magnesium sulfate ($MgSO_4$), di-potassium hydrogen phosphate(K_2HPO_4), sodium carbonate (Na_2CO_3), sodium hydroxide (NaOH), calcium chloride ($CaCl_2.2H_2O$), potassium chloride (KCl), cadmium nitrate [Cd $(NO_3)_2$.

$4H_2O$], potassium dichromate ($K_2Cr_2O_7$), nickel nitrate [Ni $(NO_3)_2.6H_2O$], sodium arsenate ($Na_2HAsO_4.7H_2O$), copper nitrate [Cu $(NO_3)_2$. $3H_2O$], lead nitrate [Pb $(NO_3)_2$], and zinc sulfate ($ZnSO_4.7H_2O$) were procured from Merck, Germany. For culture isolation, the requisite of Hori Koshi (HK) medium like peptone, and yeast extract was obtained from Hi-Media. All the chemicals used in the experiment were analytical grade and were >98% - ≥ 99.0% pure.

2.2. Sampling and isolation of the bacteria

The red mud slurry waste sample was collected from dumped sites of an alumina plant located near Muri, Jharkhand (Latitude: 23°22″ N Longitude: 85°51"E). Collected samples were brought to the laboratory and preserved at 4 °C for further analysis. The sample was highly sodic-alkaline confirmed by their pH, EC, and available Na^+ content measured by following the methods outlined by (Page et al., 1982). An alkaline-specific Hori Koshi (HK) medium (pH10.5) was used to isolate bacterial strain through an enrichment technique followed by the spread plate method. The inoculated plates were incubated at 30 °C for 48–72 h. At the end of incubation, the discrete colonies were picked up to assess and screen their metal tolerance.

2.3. Determination of maximum tolerable concentration (MTC) and other growth parameters

To determine the maximum tolerable concentration (MTC), glucose yeast extract peptone (GYP) broth was supplemented with varying concentrations of metal solution from 50 mg L^{-1} to 3500 mg L^{-1}. Approximately 1×10^6 CFU ml^{-1} cells were inoculated and kept for 48 h at 30 °C under shaking conditions (150 rpm). After incubation, the growth of the isolates was confirmed by measuring optical density at 600 nm. The bacterial isolate with the highest MTC was selected for further study. Additionally, the growth parameters were also optimized for the selected isolate by measuring tolerance to pH (4–13), temperature (20°C-55 °C), and NaCl concentration (10%–35%) (Khan et al., 2021).

2.4. Phenotypic and molecular characterization of the isolate

The colony morphology of the selected isolate was studied on a glucose-yeast extract-peptone (GYP) agar medium (pH 10.5). Gram characteristics were examined using the Gram staining procedure and subsequently visualized under a bright field microscope. Biochemical characterization viz. carbohydrate fermentation, citrate utilization, arginine production, ONPG, methyl red/Voges Proskauer test according to manufacturer's instruction (Hi-carbo KB009 kit, KB013 kit; Hi-media). For molecular identification genomic DNA was isolated following the standard protocol (Sambrook, 2001). The quality was checked on 1% agarose gel, and subsequently amplified by using 16s rDNA forward (27F) and reverse primer (1492R). Forward and reverse DNA sequencing reaction of PCR amplicon was carried out with forward primer and reverse primers using BDT v3.1 Cycle sequencing kit on ABI 3730xl Genetic Analyzer. The consensus sequence of the 16S rDNA gene was generated from forward and reverse sequence data using aligner software. The 16S rDNA gene sequence was used to carry out BLAST analysis with the NCBI GenBank database. Based on the maximum identity score first ten sequences were selected and aligned using the multiple alignment software program Clustal W. Distance matrix was generated and the phylogenetic tree was constructed using MEGA 7. Lastly, the consensus sequence was deposited to NCBI for accession number.

2.5. Preparation of dry biomass/biosorbent

The dry biomass was prepared following the method outlined by Palanivel et al. (2020). Briefly, cells were grown in HK broth medium and incubated at 30 °C for 48h. The cells were harvested at a late exponential stage by centrifugation at 8000 rpm for 15 min. For the preparation of dry biomass, the harvested cell pellets were washed thrice with PBS buffer of pH 7.4 and dried at 65 °C for 10–12 h.

2.6. Removal efficiency in the single-component system (batch adsorption study) and multi-component system

To check the removal efficiency of the biosorbent batch adsorption studies were carried out using dried biomass (biosorbent) under various parametric conditions such as pH (2–10), temperature (20°C-45 °C), adsorbent dose (1g L^{-1}-3 g L^{-1}), initial metal concentration (30–500 mg L^{-1}), contact time (15–120 min) and salinity (2%–6%) to optimize the adsorption (biosorption) process. For individual experiments, 10 ml of metal solution (Cd^{2+}, Cr^{6+}, Ni^{2+}) was incubated with bacterial biomass. The metal solution without bacterial biomass (biosorbent) was taken as the control. After biosorption, the supernatant was recovered by centrifugation at 5000 rpm for 10 min. Atomic adsorption spectroscopy (Systronics AAS 816) was used to measure the residual metal concentration in the supernatant. The efficacy of the biosorbent was quantified in terms of metal removal (%) and adsorption capacity (mg g^{-1}) using the below-mentioned formulas:

$$\text{Removal } (\%) = \frac{Ci - Ce}{Ci} \text{ X100 } \ldots\ldots\ldots\ldots\ldots \quad (1)$$

$$\text{Adsorption capacity } (Qe) = \frac{Ci - Ce}{m} \text{ X V } \ldots\ldots\ldots\ldots \quad (2)$$

where C_i and C_e are the initial concentration and residual concentration of metal (mg L^{-1}) respectively, V is the volume of the reaction mixture (L) and m is the mass of adsorbent (g).

Biosorption was also studied in ternary metal solution to assess if there is any collective or competitive effect among metals, which will impact the removal efficiency or adsorption capacity of biosorbent. The experimental setup has a combination of (Cd + Ni + Cr), (Ni + Cd + Cr), and (Cr + Ni + Cd). The concentration of the first metal ion in each combination was kept constant at 100 mg L^{-1} and the concentration of other metal ions were varied from 100 to 500 mg L^{-1}. Other parameters were kept at optimum as was obtained from a single metal system. The experimental conditions were: pH 6 for Cd^{2+}, Ni^{2+}, and pH 2 for chromium Cr^{6+}. The adsorbent dose was 3g L^{-1} with a timeframe of 120 min at room temperature (30 °C) and constant shaking at 150 rpm.

2.7. Biosorption isotherm

To assess the biosorption process isotherm models, i) Langmuir (1st, 2nd, 3rd, and 4th), ii) Freundlich, iii) Temkin, iv) Dubinin-Radushkevich; v) Elovich and vi) BET (Brauer-Emmett-teller) were used. The model analysis was carried out in R software (version 2023.09.1) using the "*PUPAIM*" (version 0.3.1) package. Langmuir isotherm describes a monolayer homogenous adsorption process while Freundlich defines a multilayer heterogeneous adsorption process (Febrianto et al., 2009; Khan et al., 2021). Temkin isotherm is a monolayer adsorption isotherm model that considers the potential impacts on the adsorption process of indirect interactions between molecules of the adsorbate. Dubinin–Radushkevich (D–R) isotherm is another model through which surface interaction between biosorbent and metal was characterized. The Elovich isotherm model describes the adsorption sites would exponentially increase with chemical reactions responsible for adsorption while BET mainly determines the multilayer adsorption process in gas systems but can also be used to establish the binding between layers in an aqueous solution owing to the molecular charges present there.

2.8. Adsorption kinetics

The adsorption rate kinetic parameters were studied by pseudo-first-order and pseudo-second-order models (Chatterjee et al., 2020). The pseudo-first-order and second-order equations are represented in Eqs. (3) and (4)

$$\ln (q_e - q_t) = \ln q_e - K_1 t \ldots\ldots\ldots\ldots\ldots\ldots \quad (3)$$

$$\frac{t}{q_t} = \frac{1}{K_2 q_e^2} + \frac{1}{q_e} t \ldots\ldots\ldots\ldots\ldots\ldots\ldots\ldots \quad (4)$$

In the pseudo-first-order equation, q_t designates the adsorption capacity (mg g^{-1}) at time t while K_1 (min^{-1}) is the equilibrium rate constant. In the case of the pseudo-second-order equation, K_2 (g $mg^{-1}min^{-1}$) is the equilibrium rate constant. The linear coefficient regression values (R^2) were evaluated and analysed to interpret the accuracy of the model by comparing the theoretical value of adsorption capacity obtained from the batch adsorption studies.

2.9. Thermodynamics analysis

For a better understanding of the adsorption behaviour of the metal ions-biosorbent at different temperatures (20 °C to 45 °C), thermodynamic parameters were assessed. The free energy of the sorption process (ΔG^0), changes in the enthalpy (ΔH^0), and entropy (ΔS^0) during the time of interaction are given by Vant -Hoff equation (Chatterjee et al., 2020).

$$\Delta G^0 = -RT\, lnK \ldots\ldots\ldots\ldots\ldots\ldots\ldots\ldots \quad (5)$$

Where k is the equilibrium constant derived from the metal concentration adsorbed on the biosorbent to the residual concentration that remains in the solution, R is the gas constant (8.314 J mol^{-1}. K^{-1}) and T is the absolute experimental temperatures. Eq (6) determines the relationship between ΔG^0 to enthalpy change (ΔH^0), and entropy change (ΔS^0).

$$\Delta G^0 = \Delta H^0 - T\Delta S^0 \ldots\ldots\ldots\ldots\ldots \quad (6)$$

Substituting Eq (5) into Eq (6) gives

$$lnk = \frac{-\Delta H^0}{RT} + \frac{\Delta S^0}{R} \ldots\ldots\ldots\ldots\ldots\ldots\ldots \quad (7)$$

From the ln$K$ vs 1/T plot, the ΔH^0 and ΔS^0 were determined.

2.10. Effect of competitive ions

The effect of competitive ions on the biosorption process was checked following (Chatterjee et al., 2020). The biosorption experiment was carried out in the presence of common cations (Na^+, K^+, Ca^{2+}, Mg^{2+}, Cu^{2+}, Pb^{2+}, Zn^{2+}) and anions (NO^{3-}, CO_3^{2-}, Cl^-, SO_4^{2-}). The biosorption was carried out under optimum conditions [3 g L^{-1} dose, 120 min, pH 6 (Cd^{2+} and Ni^{2+}) and pH 2 (Cr^{6+})]. The residual metal concentration in the solution was measured by Systronics AAS 816.

2.11. Desorption and reusability study

To carry out the desorption study the metal-laden biosorbent was treated with 0.1(N) of basic and 0.5(N) acidic solution (NaOH, Na_2CO_3, HCl, HNO_3, and H_2SO_4) following Masoudi et al. (2018). The metal-adsorbed biosorbent was washed to release any unbound metal and following treated with a desorption solution. Subsequently, the biomass harvested from the reaction mixture and desorption capacity were measured following equation:

$$\%\ \text{of desorption} = \frac{amount\ of\ metal\ desorbed}{amount\ of\ metal\ adsorbed}\ X\ 100 \ldots\ldots\ldots\ldots \quad (8)$$

The three most effective desorption solutions for three different metals were used for reusability study [(0.1(N) NaOH for Cr^{6+}, 0.5(N) HCl for Cd^{2+}, and 0.5(N) HNO_3 for Ni^{2+})]. It is a consecutive adsorption-desorption experiment up to five times. After each cycle the biomass was harvested by centrifugation, washed with distilled water, and semi-dried, to regenerate successfully for the subsequent adsorption-desorption experiment.

2.12. Microscopic and spectroscopic analysis

Field emission scanning electron microscopic analysis (FE-SEM, Zeiss Gemini; Sigma 300, Germany) was performed for metal (Cd^{2+}, Ni^{2+}, Cr^{6+}) treated and untreated biomass to visualize if there are any morphological changes. The sample was prepared following Priyadarshanee et al. (2021). Briefly, the pristine and metal-adsorbed biomasses were washed with PBS 7.4 to eliminate any unbound or loosely attached component followed by a fixation over a glass slide with 2.5% glutaraldehyde. The slides were kept at 4 °C for 12 h. The fixed slides were then dehydrated by using an increasing concentration of ethanol gradient (30, 50, 70, 80, 90%) for 10 min and finally dehydrated with absolute ethanol for 20 min. Subsequently, dehydrated samples were coated with gold for 15 min and observed under FESEM at a stable voltage of 5 KeV. The elemental analysis between treated and pristine biomass was done by performing energy-dispersive X-ray spectroscopy (EDS, INCA 250, UK) which was coupled with FESEM. The involvement of the surface-active functional group was investigated using Fourier transform infrared spectroscopy. The spectra of before and after metal interaction were recorded within the wavenumber range between 400 and 4000 cm^{-1} using an FT-IR spectrometer (PerkinElmer, USA, Model: Spectrum 400 FT-IR/FIR Spectrometer).

2.13. Statistical analysis

All the experiments executed in triplicates were expressed as mean ± SD. The statistical analysis was performed using GraphPad (Prism Version 7.00). Two-way analysis of variance (ANOVA) followed by Tukey's multiple comparisons test was conducted to evaluate significant differences among parameters of batch adsorption. Further, for batch adsorption with variable pH and metal concentration and desorption studies, one-way ANOVA following Sidak's multiple comparisons test was carried out. One-way ANOVA following Dunnett's multiple comparisons test was assessed for reusability study. For the entire study, $p < 0.05$ was referred statistically significant value.

2.14. Speciation modelling using visual MINTEQ 4.0 software

The equilibrium Cd^{2+}, Ni^{2+} and Cr^{2+} speciation was predicted using Visual MINTEQ 4.0 (4.05) software (Gustafsson, 2023). The model parameters and input components have been depicted in Table S1.

3. Results and discussion

3.1. Isolation, phenotypic characterization, maximum metal tolerance, and molecular identification

The collected red mud sample was red in colour and semisolid in texture. The pH ranged between 10.5 and 13.5 along with high electrical conductivity of 4.6–13.6 mS cm^{-1} and Na^+ (0.9%–6.5%) concentration. The free and soluble soda in form of sodalite may be the root cause of this alkalinity of red mud (Dey and Paul, 2021). It also consisted of numerous heavy metals like, Cr, Cd, Ni, Pb, etc.; listed in Table S2. Other physicochemical characteristics viz., % organic C, % of total Kjeldahl N (TKN), cation exchange capacity (CEC), sodium, potassium, calcium, and magnesium are also recorded in Table S2. High alkalinity, elevated Na^+ concentration, and low nutrient availability resulted in sparse vegetation in red mud which may be the reason for its poor organic carbon and available nitrogen content (Courtney and Xue, 2019; Dey

and Paul, 2021). The alkaline environment of red mud acts as a sink of alkaliphilic bacteria, as found in the present study, which also conforms with the findings of Agnew et al. (1995); Mishra et al. (2016); and Dey (2021). Five morphologically distinct metal-tolerant bacterial colonies were isolated and identified. Among them, RM16 showed maximum tolerance to the subjected heavy metals (Cd^{2+}, $Ni^{2+,}$ and Cr^{6+}) depicted in Fig. S1. Such high metal tolerance may be attributed to different coping mechanisms such as intracellular accumulation, biosorption, efflux, redox reaction, etc, (Roy et al., 2023). Based on MTC, RM16 was selected for further investigation. The gram-positive bacterial colony is yellow-coloured, gummy, flat, and marginally smooth. The phenotypic and biochemical characteristics of the isolates are listed in Table S3.

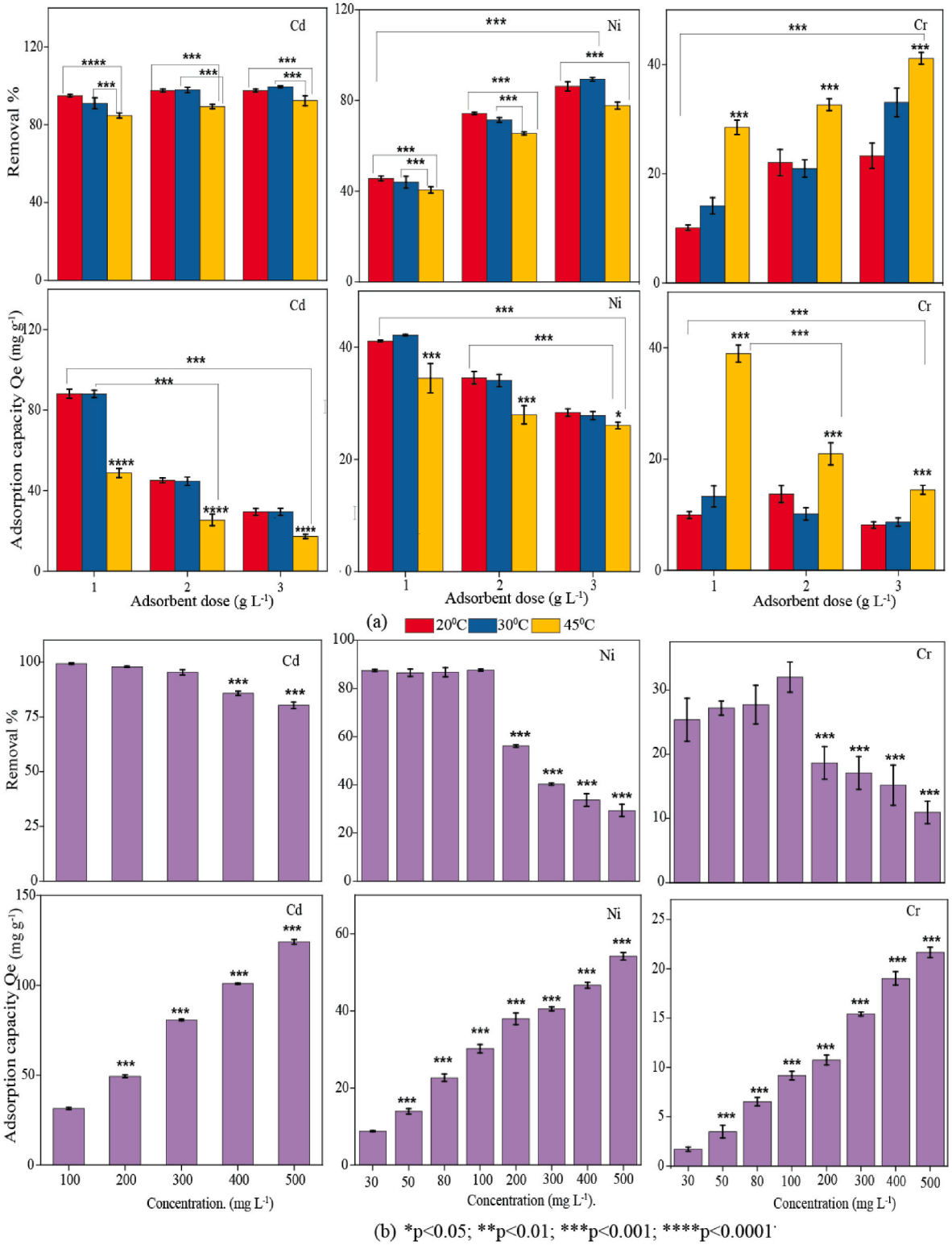

Fig. 1. (a) Effect of biomass dose on the removal and adsorption capacity of Cd^{2+}, Ni^{2+}, and Cr^{6+} concerning temperature. (b) Effect of initial concentration on removal and adsorption capacity of Cd^{2+}, Ni^{2+}, and Cr^{6+}.

The optimum growth conditions of the isolate were observed at pH 10.5, 30 °C temperature, and 10% NaCl concentration (Fig. S1). However, it was resistant to a wide range of pH (pH 8–13), temperature (20 °C to 50 °C), and NaCl concentration (10%–30%). The physiological profile indicates its ability to sustain itself in a hostile environment (Shylla et al., 2021). Considering multiple metal tolerance RM16 exhibited a significant tolerance to As^{5+}, and Cu^{2+} in addition to Cd^{2+}, $Ni^{2+,}$ and Cr^{6+} (Fig. S1). Tolerance against a wide range of metals may come from metalloproteins (metallothionine) that possess a high binding affinity for various metals like Cd^{2+}, and Cu^{2+} (Giovanella et al., 2020). In general, Cr tolerance is attributed to two mechanisms either chromate efflux from the cell or enzymatic reduction, while Ni resistance is commonly mediated by an efflux pump (Das et al., 2016). Recently plasmid-borne *cad, czc* operon, and *nre* operon have been reported to confer Cd and Ni resistance in *Staphyllococcus* spp. *Pseudomonas aeruginosa* and *Achromobacter xylosoxidans* 31A (Chakraborty and Das, 2014; Grass et al., 2005). In the case of As, the enzyme machinery arsenic reductase may be responsible for such high tolerance (Dey et al., 2016).

According to 16srDNA-based homology, the isolate showed maximum similarity with *Bacillus xiamenensis* (accession no. NR_148244.1) and was identified as *Bacillus xiamenensis* ISIGRM16 (Fig. S2). The isolate was submitted to NCBI under accession number OP243450. A study by Yahaghi et al. (2018), reported that *Bacillus* is the predominant species in metal-contaminated soil with high metal tolerance. Likewise, the present finding of the indigenous halo-alkali tolerant *Bacillus xiamenensis* ISIGRM16 with high MTC could be a potential candidate for heavy metal remediation purposes.

3.2. Optimization of the biosorption conditions

3.2.1. Effect of biomass dose

The impact of biomass dose on metal sequestration (Cd^{2+}, Ni^{2+}, Cr^{6+}) was studied using a variable range of biomass dose from 1g L^{-1} to 3g L^{-1} at three distinct temperatures i.e., 20 °C, 30 °C, and 45 °C for 2 h with 100 mg L^{-1} metal solution. The removal efficiency significantly increased with increasing biomass dose whereas biosorption capacity decreased (Fig. 1a). This may be due to an increment in the surface area and available active site in the medium (Cherono et al., 2021). 99.55 % ± 0.51 Cd^{2+} was removed at 30 °C while the removal efficacy significantly decreased to 92.33% ± 2.4 ($p < 0.0001$, two-way ANOVA, Tukey's multiple comparison test) when temperature rises to 45 °C. The removal of Ni^{2+} was a maximum of 89.37% ± 0.78 at 30 °C and dropped down significantly ($p < 0.0001$) at 45 °C (77.72% ± 1.5). Formerly Cd^{2+} and Ni^{2+} adsorption by an extremophilic *Geobacillus* sp. was investigated by Özdemir et al. (2009) who reported 82.2% and 53.2% removal respectively at 100 mg L^{-1} of initial concentration implying that the investigated species of our study has greater efficiency. In contrast, Cr^{6+} adsorption was highest at 45 °C i.e., 41.15% ± 1.06. All three metals were maximally removed at 3g L^{-1} dosage and considered as the optimum dose, a further increase in biomass dose had no significant effect on removal per cent. It was found that biosorption capacity (Q_e) was inversely related to biomass dose while directly related to the per cent of removal. The biosorption capacity for three HMs was in the order: of Cd^{2+} >Ni^{2+} >Cr^{6+}. At 1g L^{-1} biomass dose, the biosorption capacity was 88.07 mg g^{-1}, 42.12 mg g^{-1}, and 38.95 mg g^{-1} for Cd^{2+}, Ni^{2+}, and Cr^{6+}respectively, while 3g L^{-1} dose significantly ($p < 0.0001$) reduced the metal uptake (biosorption capacity) (Fig. 1a). This can be attributed to the inadequacy of metal ions at high biomass doses to completely cover the available binding site, however, overlapping and aggregation with increased biomass may also be the fact for lower uptake capacity at higher doses (Nuhoglu and Malkoç, 2009; Verma et al., 2014).

3.2.2. Influence of initial metal concentration

The effect of metal concentration on the biosorption process was important to assess because wastewater streams frequently contain high concentrations of heavy metals. To investigate that, the initial metal concentration for Cd^{2+} was selected from 100 mg L^{-1} to 500 mg L^{-1} while 30 mg L^{-1} to 500 mg L^{-1} for Ni^{2+} and Cr^{6+}. The results depicted in Fig. 1b describe that removal per cent was inversely related to metal concentration while directly related to biosorption capacity (Q_e) at a fixed biosorbent dose (3g L^{-1}). The uptake capacity was maximum at the highest metal concentration i.e., 500 mg L^{-1} which could be attributed to a slower diffusivity of the metal ions by intra-particular diffusion at higher concentrations (Skodras et al., 2008). Also, higher driving force at higher concentrations may facilitate the adsorption (biosorption) capacity of biosorbent (Masoudi et al., 2018). The biosorption capacity of the biomass was in the order Cd^{2+} (124.11 ± 1.26 mg g^{-1}) > Ni^{2+} (54.20 ± 0.99 mg g^{-1}) > Cr^{6+} (21.65 ± 0.5 mg g^{-1}). In contrast, the depreciation in removal per cent at high metal concentrations is due to the saturation of the adsorption site (Gupta et al., 2019). At lower concentrations, the binding site of metal ions is adequate, whereas, with increasing concentration, competition among metal ions occurs for available binding sites that significantly decrease per cent removal at high concentrations (Oves et al., 2013; Gupta et al., 2019).

3.2.3. Effect of contact time on biosorption concerning temperature

Any adsorbent's ability to facilitate adsorption is necessary to be validated through reaction time. In addition to that the temperature during the reaction time could have an impact on the adsorption process as well. The findings revealed that equilibrium was achieved after 60 min of interaction for Cd^{2+} and 90 min for Ni^{2+} and Cr^{6+} (Fig. 2 a-c). However, removal of metal was rapid at initial 15–30 min, then gradually improved up to equilibrium at which metal sequestration achieved a saturation state. Subsequently, the removal remained constant may be because more vacant sites are available at initial state causing enhanced biosorption which is further slowed down due to exhaustion of residual surface site and repulsive force between adsorbent-adsorbate interaction (Saravanane et al., 2002). The removal was highest for Cd^{2+} (98.14% ± 0.22) followed by Ni^{2+} (87.81% ± 0.14) and Cr^{6+} (41.76% ± 1.63). Possible reason for the maximum removal at equilibrium includes three stages, an initial rapid binding of metal ions or mass transfer followed by intra-particular diffusion, and lastly sorption of ions (Quintelas et al., 2009). The rising of temperature from 20 °C to 45 °C significantly decreased the removal ($p < 0.0001$) of Cd^{2+} (from 98.17% ± 0.22–90.27% ± 1.9) and Ni^{2+} (from 87.81% ± 0.14–77.67% ± 0.9). Contrastingly, Cr^{6+} removal greatly improved from 33.95% ± 2.3–41.76% ± 1.63 ($p = 0.0010$) demonstrating its endothermic adsorption process previously reported by Chatterjee et al. (2022).

3.2.4. Effect of pH on biosorption

pH is an important governing factor in the adsorption process affecting the heavy metal speciation, degree of ionization of adsorbate during reaction time, and surface chemistry of the biosorbent (Gupta et al., 2019; Tuomikoski et al., 2021). Thus, the impact of H^+ ions on the biosorption process was important to evaluate the removal efficacy of the biosorbent within a wide range of pH (Fig. 2d). The experiment was conducted covering acidic to basic range (2,4,6,8,10) to obtain the optimum pH for biosorption using a 3g L^{-1} biomass dose in 100 mg L^{-1} metal solution at room temperature (30 °C). The optimum pH was found to be at 6 for maximum removal of Cd^{2+} (98.24% ± 1.0.) and Ni^{2+} (86.30% ± 0.2). However, the biosorption significantly ($p < 0.0001$) dropped in both acidic and basic pH for these positively charged cations. At pH 2 the removal was lowest (15.40% ± 1.5 for Cd^{2+} and 1.6% ± 0.7 for Ni^{2+}) which attributed to competitive effects between protons (H^+) and metal ions. The apparent dominance of H^+ ions in the solution restricted the adsorption of metal ions owing to repulsive forces (Gupta et al., 2019; Manasi et al., 2014). At > pH 8 Cd^{2+} biosorption significantly ($p = 0.0018$) decreased (85.25% ± 1.3 at pH 10) which seems to be the result of Cd ion precipitation due to the abundance of OH^- ion in the solution (Masoudi et al., 2018). Ni^{2+} biosorption started to reduce >6 (77.53% ± 0.89 at pH 8 and 63.44% ± 0.9 at pH10; $p < 0.0001$)

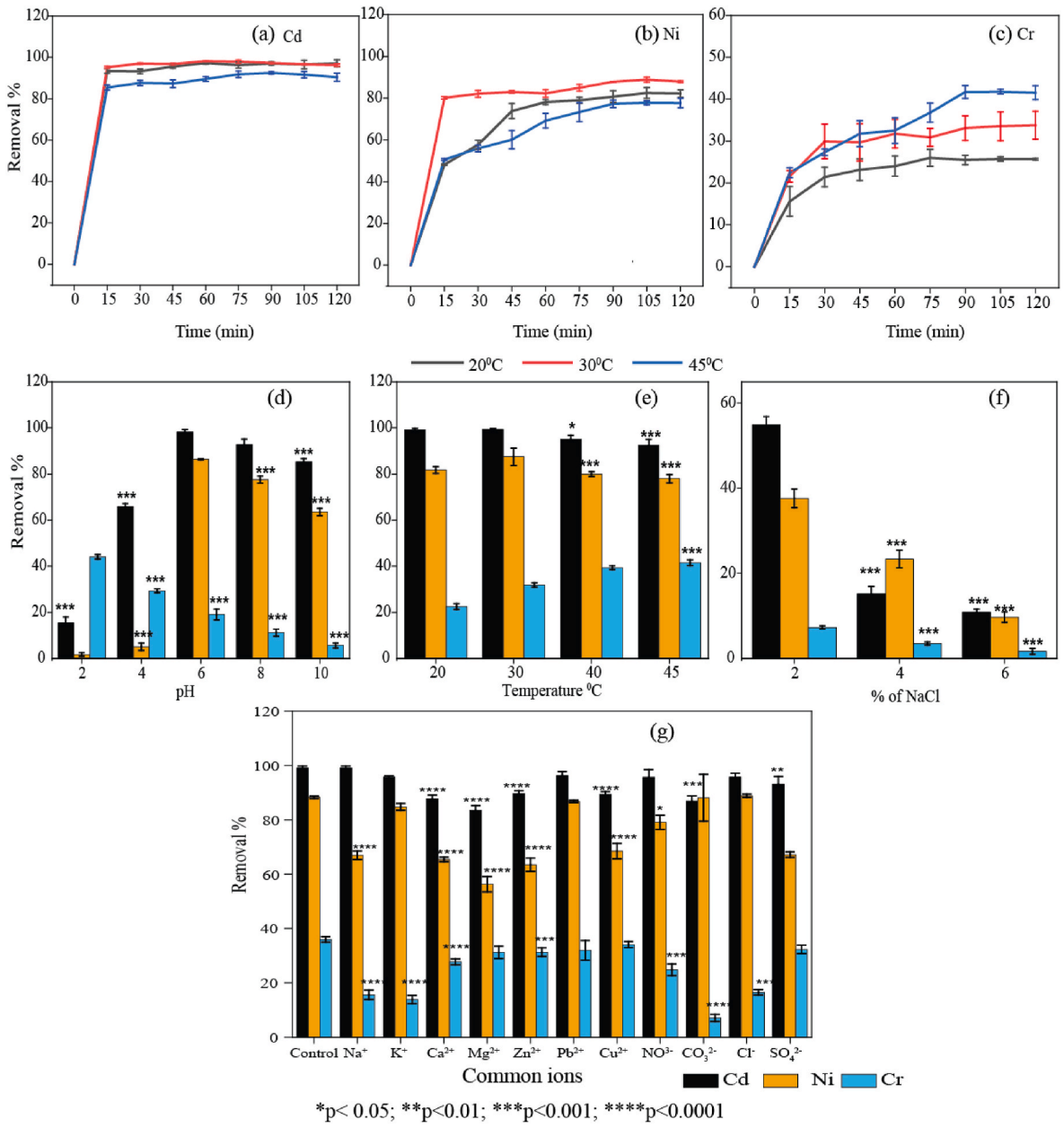

Fig. 2. (a–c) Effect of time, (d) pH, (e) temperature, and (f) salinity (% NaCl) on the removal of Cd^{2+}, Ni^{2+}, and Cr^{6+}. (g) Influence of co-occurring ions on the removal of Cd^{2+}, Ni^{2+}; and Cr^{6+}.

since Ni began to precipitate after pH 6 (Hoseini et al., 2020). Our observation for Cd^{2+} and Ni^{2+} is in line with the investigation done by Özdemir et al. (2009); Oves et al. (2013), and Wen et al. (2021). In contrast, maximum removal of Cr^{6+} was observed at pH 2 (44.03% ± 0.96). As chromium produces negatively charged $HCrO_4^-$, $Cr_2O_7^{2-}$, CrO_4^{2-}, $Cr_4O_{13}^{2-}$ and $Cr_3O_{10}^{2-}$ in an aqueous solution, it was more adsorbed when the surface of the biosorbent was protonated and consequently showed excellent removal at pH 2 (Verma et al., 2014). Increasing the pH from 2 to 4 significantly reduced the removal from 44.03% ± 0.96–29.35% ± 0.89 ($p < 0.0001$) and at pH10 the removal was 5.58% ± 1.04 ($p = 0.0063$). Increment in pH induces the hydroxyl anion and negative charges of biosorbent therefore decreasing the Cr^{6+} removal at high pH (Verma et al., 2014).

3.2.5. *Effect of temperature on biosorption*

The magnitude of temperature affects the interaction between metal ions – biosorbent complex and influences the surface moieties of biomass (Chakravarty and Banerjee, 2012). The result depicted in Fig. 2e showed, that high temperatures (40 °C and 45 °C) significantly ($p < 0.001$) decrease Cd^{2+} and Ni^{2+} removal while favours Cr^{6+} removal. The removal per cent of $Cr^{6+}$was highest at 45 °C (41.51% ± 1.1; $p = 0.0001$) which can be attributed to increment in the kinetic energy of $Cr_2O_7^-$, the predominant species in acidic conditions, as well the increase in contact of these ions with biosorbent (Kamranifar et al., 2019). Conversely, significant decline was observed from 99.34% ± 0.21 (30 °C) to 92.39% ± 2.01 (45 °C) ($p = 0.0099$) for Cd^{2+}, and 87.43% ± 1.2 (30 °C) to 77.93% ± 1.2 (45 °C) ($p = 0.0043$) for Ni^{2+}. Such reduction may be due to various parameters: elevated escaping tendency of metal ions from aqueous to bulk phase, increased solubility of the metal ions at moderately high temperature, weakening of the adsorptive forces between the active site of biosorbent and metal ions in solution (Gupta et al., 2019; Gupta et al., 2019).

3.2.6. Effect of NaCl concentration on biosorption

NaCl concentration can be as impactful as other parametric conditions for the biosorption process. Cd^{2+} and Ni^{2+} were removed by the biomass up to 4% of NaCl concentration (Fig. 2f), however, the removal was maximum at 2% NaCl concentration (54.85% ± 1.3 for Cd^{2+} and 37.61% ± 1.2 for Ni^{2+}). Further increase in NaCl concentration considerably reduced the removal efficiency ($p < 0.0001$). The findings are in line with Mohapatra et al. (2019) who observed the removal of another divalent cation Pb by *Bacillus* sp. under NaCl concentration. Removal of Cr^{6+} was found to be negligible in saline solution.

3.3. Equilibrium studies

3.3.1. Adsorption isotherm

Adsorption isotherms determine the interaction between metal ions and biosorbents thus providing information to understand the mechanism of the adsorption process. It illustrates the equilibrium state of metal ions at the surface-liquid interface at a constant temperature (Verma et al., 2014). Each model put light on the mechanistic insight of the adsorption process at different metal ion concentrations (30–500 mg L^{-1} for Cr^{6+} and Ni^{2+} and 100–500 mg L^{-1} for Cd^{2+}). The model parameters are tabulated in Table 1 and the best-fitting model is determined by the linear regression coefficient (R^2) value (Figs. S3, S4, S5). Langmuir isotherm 1st and 2nd linear model was found to be the best fitted for Ni^{2+} ($R^2 \geq 0.97$) and Cr^{6+} ($R^2 \geq 0.95$) owing to their high R^2 values. This suggests that a monolayer pattern of biosorption occurred on the biosorbent surface along with uniformly distributed sorption energy. Since Langmuir isotherm theoretically predicts the homogeneous nature of the biosorbent surface with a uniform distribution of binding sites sharing indistinguishable affinity that facilitates absolute monolayer adsorption of metals (Verma et al., 2014; Chatterjee et al., 2022). The maximum yielded adsorption capacity (Q_{max}) was 52.49 mg g^{-1} and the coefficient of adsorption energy K_L (L mg^{-1}) was 0.04. The dimensionless R_L 0.2 confirms the favourability of the Ni^{2+} adsorption onto biomass surfaces [favourable adsorption ($0 < RL < 1$), unfavourable adsorption ($RL > 1$), linear ($RL = 1$), or irreversible ($RL = 0$).]. In the case of Cr^{6+} maximum adsorption capacity Q_{max} (mg g^{-1}) was 85.9 and the R_L value (0.91) lies less than 1 suggesting a favourable adsorption process. On the other hand, Freundlich isotherm was the best fit for Cd^{2+} indicating bonding energy-driven multilayer heterogenous adsorption of metal ions onto the biomass surface due to higher $R^2 \geq 0.98$, describing the equilibrium state. The Freundlich constant K_f related to adsorption capacity was 31.99 and 1/n adsorption intensity derived from slope and intercept of Log Q_e vs Log C_e plot is less than 1 securing a favourable interaction between Cd^{2+} and biosorbent. Temkin isotherm determines the adsorption heat of all the molecules in the layer decrease linearly and based on electrostatic interaction (Eldin et al., 2016). In the present study except for Cd^{2+}, the other metals poorly fit with the model. The R^2 for Cd^{2+} was 0.97 while for Ni^{2+} and Cr^{6+} it was 0.92 and 0.94 respectively. The isotherm constants B and K_T were determined from the intercept and slope of the Q_e vs ln C_e plot. The calculated value for Cd^{2+} equilibrium binding constant K_T (L mg^{-1}) was 20.54 and B (J mol^{-1}) was 3.52. Elovich and BET isotherms were also found to have good fitness for Cd^{2+} ($R^2 \geq 0.96$ and $R^2 \geq 0.95$ respectively) compared to Ni^{2+} and Cr^{6+} (Table 1). Elovich demonstrates sorption site increment with exponential adsorption, implying multilayer adsorption. Similarly, BET isotherm determines that, adsorption occurs due to the attraction of adsorbate onto the surface of biosorbent in a random distribution, indicating multilayer formation of adsorbed particles. The D-R isotherm model is independent of Langmuir or Freundlich isotherm model and commonly describes the sorption mechanism of a single solute system(Dubinin et al., 1947). In the present study, all the metals barely follow the D-R isotherm due to their poor regression coefficient.

Table 1
Adsorption models for biosorption of Cd^{2+}, Ni^{2+}, and Cr^{6+}.

Adsorption models (Linear Models)	Parameters	Test Metals		
		Cd^{2+}	Ni^{2+}	Cr^{6+}
Langmuir isotherm first form	Q_{max} (mg g^{-1})	126.51	52.49	34.71
	K_L	0.15	0.04	0.003
	R_L	0.07	0.2	0.78
	R^2	0.97	0.97	0.86
Langmuir isotherm second form	Q_{max} (mg g^{-1})	99.8	58.20	86.00
	K_L	0.39	0.05	0.001
	R_L	0.03	0.16	0.91
	R^2	0.94	0.94	0.95
Langmuir isotherm third form	Q_{max} (mg g^{-1})	108.25	47.67	26.40
	K_L	0.32	0.08	0.005
	R_L	0.03	0.11	0.68
	R^2	0.78	0.74	0.55
Langmuir isotherm fourth form	Q_{max} (mg g^{-1})	114.11	52.09	35.82
	K_L	0.27	0.06	0.003
	R_L	0.04	0.14	0.78
	R^2	0.78	0.74	0.55
Freundlich isotherm	K_f (L mg^{-1})	31.99	9.122	0.29
	1/n	0.30	0.30	0.72
	R^2	0.98	0.80	0.94
Temkin isotherm	B (J mol^{-1})	20.54	8.20	6.177
	K_T (L mg^{-1})	3.526	1.33	0.05
	R^2	0.97	0.92	0.94
Dubinin-Radushkevich isotherm	Q_e	89.04	39.77	13.25
	E (KJmol^{-1})	1083.91	329.68	56.42
	β (mol^2/K^2J^2)	4.25E-07	4.60E-06	1.50E-04
	R^2	0.66	0.87	0.78
Elovich isotherm	Q_{max} (mg g^{-1})	30.25	13.22	23.02
	K_e	2.4	0.63	0.005
	R^2	0.96	0.79	0.65
BET- isotherm	Q_m (mg g^{-1})	−6755.36	−716.05	−41.68
	C_S	−400	0.12	−354.08
	C_{BET}	0.02	−363.26	0.90
	R^2	0.95	0.89	0.07

3.3.2. Adsorption kinetics

Adsorption kinetics plays a vital role in designing sorption experiments. It is important to assess the mechanistic approach to interaction and the rate of adsorption process during mass transfer and chemical interaction (Mohapatra et al., 2019). The kinetic model parameters are presented in Table 2. The studied biosorption data fit with pseudo-second-order due to its high coefficient (R^2 closer to 1) for Cd^{2+}, Ni^{2+}, and Cr^{6+} (Fig. 3 a-f). Furthermore, pseudo-second-order had shown the best agreement for calculated ($Q_{e.cal}$) and experimented ($Q_{e.exp}$) adsorption capacity. Whereas the $Q_{e\cdot cal}$ of pseudo-first-order showed a large deviation with our experimental data as well the poor R^2 values rejecting the model for the present study (Table 2). The best fitness of the pseudo-second-order model to the empirical data deducing that the rate-limiting step in biosorption was the chemisorptive valence force caused due to sharing or exchange of electrons between biosorbent and adsorbate (metal ion), complexation, coordination, and/or chelation (Verma et al., 2014).

3.4. Thermodynamic investigation

The values of Gibbs free energy (ΔG^0), enthalpy (ΔH^0), and entropy (ΔS^0) were calculated from the lnK vs 1/t plot (Fig. 3 g-i) and summarised in Table 3. Thermodynamic analysis provides an extensive interpretation concerning to adsorption process by determining its nature (exothermic or endothermic), spontaneity, and favourability (Mekonnen et al., 2015). As per the first law of thermodynamics, it is postulated that energy cannot be generated or lost and entropy is the only driving force in an isolated system (Nuhoglu and Malkoç, 2009).

Table 2
Kinetic models for biosorption of Cd^{2+}, Ni^{2+}, and Cr^{6+}.

Kinetic Models		Cd^{2+}			Ni^{2+}			Cr^{6+}		
		20 °C	30 °C	45 °C	20 °C	30 °C	45 °C	20 °C	30 °C	45 °C
$Q_{e,\ exp}$ (mg g^{-1})		31.42	31.16	30.01	23.63	29.3	23.17	7.5	8.67	13.68
	$Q_{e,\ cal}$ (mg g^{-1})	2.39	0.66	1.61	5.34	2.27	5.21	1.55	1.13	2.88
Pseudo-first-order	K_1 (min^{-1})	−0.0006	−0.0002	-5.9×10^{-5}	-9E-05	−0.0002	-3.5×10^{-5}	−0.0003	−0.0001	−0.0002
	R^2	0.80	0.70	0.11	0.14	0.68	−0.08	0.52	0.48	0.59
Pseudo-second-order	$Q_{e,\ cal}$ (mg g^{-1})	31.22	31.02	30.35	29.3	29.8	28.32	8.76	10.04	69.63
	K_2 (g $mg^{-1}min^{-1}$)	0.083	0.34	0.054	0.005	0.024	0.004	0.052	0.043	0.0002
	R^2	0.99	0.99	0.99	0.99	0.99	0.98	0.99	0.99	0.99

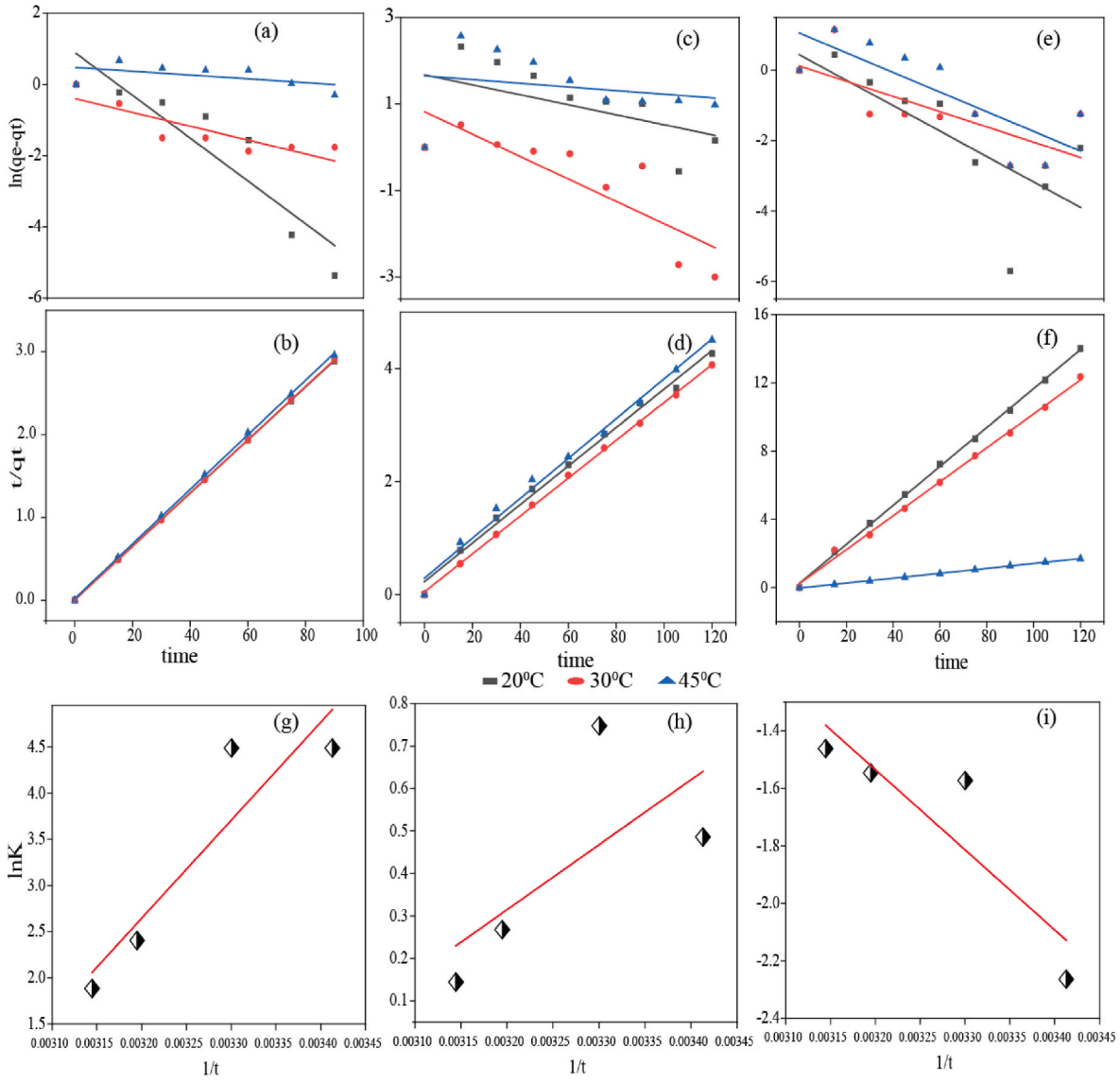

Fig. 3. Adsorption kinetics plots of biomass-biosorbent (pseudo-first-kinetics and pseudo-second-order kinetics) for (a–b) Cd^{2+}, (c–d) Ni^{2+}, (e–f) Cr^{6+}.The lnK vs 1/t plot against adsorption of (g) Cd^{2+}; (h) Ni^{2+}; and (i) Cr^{6+} (Thermodynamic study).

Hence, ΔG^0, ΔH^0, and ΔS^0 are the most genuine parameters to interpret an adsorption process. The negative ΔG^0 value of Cd^{2+} and Ni^{2+} directs the spontaneous nature of the process and with rising temperature, the decreasing value of ΔG^0 indicates unfavourable biosorption at higher temperatures while in Cr^{6+} the positive ΔG^0 demonstrates the non-spontaneous nature of biosorption. A similar type of non-spontaneous behaviour was reported in metal and dye biosorption by plant biomass (Amin et al., 2017). However, the non-spontaneity was decreased when the temperature was raised to 45 °C. The negative ΔH^0 and ΔS^0 declare the exothermic nature of the reaction where randomness decreased at the solid/liquid interface throughout the biosorption process of Cd^{2+} and Ni^{2+} and also demonstrates that biosorption decreased on the successive increase in temperature. Contrastingly, the positive ΔH^0 and positive ΔS^0 imply the endothermic reaction process with increased randomness at the solid/suspension interface during the biosorption of Cr^{6+}.

Table 3
Thermodynamic parameters for Cd^{2+}, Ni^{2+} and Cr^{6+} adsorption.

Test Metal	Temperature (^{0}C)	Temperature (K)	ΔG° (kJ. mole^{-1})	ΔH° (kJ. mole^{-1})	ΔS° (J. mole^{-1}. K^{-1})
Cd^{2+}	20 °C	293	−10.934	−88.22	−260.31
	30 °C	303	−11.307		
	40 °C	313	−6.257		
	45 °C	318	−4.979		
Ni^{2+}	20 °C	293	−1.183	−12.72	−38.09
	30 °C	303	−1.883		
	40 °C	313	−0.697		
	45 °C	318	−0.381		
Cr^{6+}	20 °C	293	5.514	23.16	61.35
	30 °C	303	3.961		
	40 °C	313	4.022		
	45 °C	318	3.864		

3.5. Competitive biosorption and interactive behaviours among metals (Cd^{2+}, Ni^{2+}, Cr^{6+}) in ternary system

The removal per cent and biosorption capacity for all three metals in the ternary system are depicted in Fig. 4 a-b. As shown in Fig. 4 a-b the removal per cent of Cd^{2+}, $Ni^{2+,}$ and Cr^{6+} decreased ($p < 0.0001$) in presence of co-ions compared with the single ion situation. Including this, when the co-ion concentration increased from 100 to 500 mg L^{-1} without changing the target metal concentration, the removal per cent and biosorption capacity (also adsorption capacity, Q_e) of biomass both declined significantly ($p < 0.0001$). For instance, the per cent of Cd^{2+} removed in the presence of Ni^{2+} and Cr^{6+} decreased to 84.33% ± 0.61 (99.55 % ± 0.51 in a single ion system), and when the concentration of Cr^{6+} and Ni^{2+} increased up to 500 mg L^{-1}, the removal decreased to 42.19% ± 0.8 ($p < 0.0001$). Correspondingly, the biosorption capacity for ions decreased in the ternary system due to co-adsorption. The results validate that the co-cations in the system competed severely for the adsorption site, which strongly influences, and reduces the biosorption capacity in the ternary system (Aksu et al., 1999). Progressive interference of ions may take place due to overlapping of the binding site, however, many other parameters can also influence the adsorption preference such as pH, temperature, surface characteristics of adsorbent, metal properties like electronegativity, ionic radius, electronic configuration, etc. (Jain et al., 2015). Interestingly, Ni^{2+} was found to be the most consistently adsorbed metal even at a high concentration of the presence of other ions (Fig. 4b). This can be attributed to its smallest hydrated radius along with greater electronegativity which helps it to make a strong attraction with the surface of biosorbent.

The selectivity of biosorbent for Cd^{2+}, $Ni^{2+,}$ and Cr^{6+} in a ternary system can be expressed more classically by calculating the relative adsorption capacity % (R_i) proposed by Chang and Chen (1998). Precisely it is the ratio of the adsorption capacity for one ion along with the existence of the other ions, to the adsorption capacity for that same ion when exists alone in the solution. The R_i percentage was used to determine whether the interactions among ions in ternary systems were antagonistic, synergistic, or non-interactive. R_i >100% indicates the synergistic behaviour of metal, while R_i <100% denotes the antagonistic relations and $R_i = 100$ validates non-interactive behaviour. In the present study, Ni^{2+} had the highest relative adsorption capacity (R_i) 92.57% followed by Cd^{2+} 90.66%, and Cr^{6+} at 82.46%. The calculated R_i <100% demonstrating that they are antagonistic to each other may be due to the screening effect of metals present in the trio-mixture (Sağ and Kutsal, 1996).

Additionally, the Visual MINTEQ 4.0 (4.05) software model was run in order to determine the chemical speciation of the metals in the ternary solution (Fig. S6, S7 and S8). Output from visual MINTEQ showed that divalent cations (Cd^{2+} and Ni^{2+}) were the most predominant species in the solution occupied >99%, and Cr was mainly present as $CrOH^+$ (>80%) at both pH 6 and 2. There was also existence of a trace amount of $NiOH^+$ (approx. 0.02%) and moderate amount Cr^{2+} (approx. 15%–16%). The speciation remained the same even after the increase in co-ion concentration, however, the activity of the ionic species altered at high co-ion concentrations. Two divalent cationic species (Cd^{2+} and Ni^{2+}) compete harder for the adsorption site with increased co-ion concentration, which is consistent with our % removal and adsorption capacity (Q_e) data obtained from the biosorbent efficacy in ternary solution. Moreover, the cationic speciation in aqueous solution was found to be advantageous for the biosorption owing to the presence of a negatively charged functional group on the surface of the biosorbent. Such an assertion is supported by the FTIR data obtained for the ternary solution.

3.6. Influence of co-occurring ions

The results, shown in Fig. 2g demonstrate that the presence of most of the cations significantly affected the removal of Ni^{2+}, while anions were found to be insignificant except NO^{3-} and SO_4^{2-}. Biosorption of Cd^{2+} remained unaffected in the presence of K^+, Pb^{2+}, NO^{3-}, Cl^- and but in the case of Cr^{6+} a contrasting result was obtained where the presence of cations had negligible effect while anions had a highly significant impact ($p < 0.0001$) on removal. Inclusively, the removal efficacy of biosorbent was satisfactory for both Cd^{2+} and Ni^{2+}, while the result for Cr^{6+} was not very impactful. Even if the removal efficacy lowered in terms of statistical significance in some cases nevertheless overall removal percentage is greater than 80% for Cd^{2+}, and more than 60% for Ni^{2+} is decent for remedial purposes.

3.7. Pre and post-sorption characteristics of biosorbent

FE-SEM image clearly illustrated the topological difference before and after metal interaction (Figs. 5 and 6). The surface of the biosorbent appeared to be smooth, rod-shaped, dense, and shiny before metal interaction (Fig. 5 a-j) while after metal adsorption, the surface appeared to be rough, contracted and the adhesion of layers was caused owing to the action of metals. The crystal-like structure on the cell surface is possibly from the metal aggregates deposited on the cell surface (Fig. 6 a-m). A similar kind of crystal formation was corroborated by Wen et al. (2021) in lactic acid bacteria after metal sorption. The aggregation of cells may arise from extra polymeric substances. EDS spectra recorded the presence of carbon, hydrogen, nitrogen, phosphorus, sodium, calcium, and potassium coming from the cell wall component (Fig. 5 k-l). Unabsorbed spectra did not indicate metal's presence while the adsorbed one indicated the presence of Cd^{2+}, Ni^{2+}, and Cr^{6+}(Fig. 6 n-o). The adsorption percentage on the cell surface was Ni^{2+} >Cd^{2+} >Cr^{6+}, which supports the findings, obtained in tri-metal adsorption.

FTIR analysis of pristine and metal-adsorbed biomass confirms the immobilization of metal on the biomass surface (Fig. 4e). The peak around 3400 cm^{-1} is the stretching vibration of the N–H bond of amino group and an indication of –OH group (Özdemir et al., 2009). The linear stretching around 2900 cm^{-1} elucidates the asymmetric stretching of γC-H bond of the –CH_2 group combined with the aliphatic methylene group. Other IR spectra of pristine biomass are as follows: The peak at 1638 cm^{-1} specifies the γC=O of amide I; the peak at 1549 cm^{-1} designates γNH/γC=O bond of amide II indicates the presence of carboxyl group (Quintelas et al., 2009); peak at 1081 cm^{-1} assigned for -C-O stretching vibrations; peak at 1400 cm^{-1} for P═O stretching vibration and may come from phosphoric acid, peak at 1232 cm^{-1} for C–N stretching vibration of the saccharide; peak at 400–1000 possibly the bending vibration within the polysaccharide molecule and near 599 ascribed to the deformation of modes of C–C═O groups in polysaccharides (Wiercigroch et al., 2017). Shifts in the peak positions of adsorbed biomass were evidenced which fairly defines the involvement of functional groups in adsorption. The peak near 1638 cm^{-1} was shifted to 1639 cm^{-1}, 1641 cm$^{-1,}$ 1618^{-1} for Ni^{2+}, Cd^{2+}, and Cr^{6+} respectively.

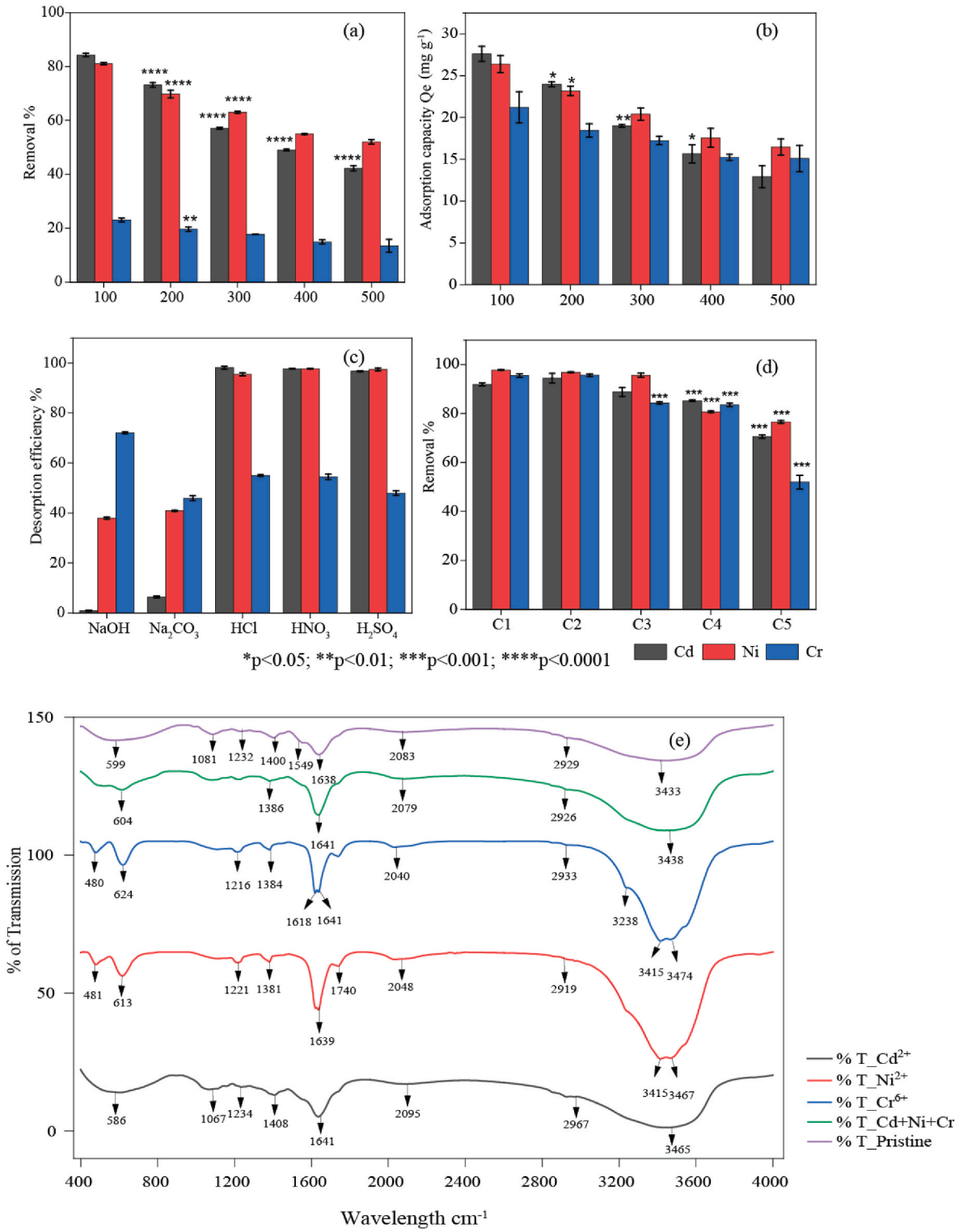

Fig. 4. (a) Effect of co-ion concentration on per cent removal of Cd^{2+}, Ni^{2+}, Cr^{6+} by *B. xiamenensis* ISIGRM16 (biosorbent) in ternary solution; (b) Effect of co-ion concentration on adsorption capacity of *B. xiamenensis* ISIGRM16 (biosorbent) in ternary solution; (c) Effect of different acidic and basic regenerative medium for desorption of Cd^{2+}, Ni^{2+}; and Cr^{6+}, (d) Reusability prospect of the biosorbent after five consecutive adsorption-desorption cycles. (e) FT-IR spectral analysis of *B. xiamenensis* ISIGRM16 (biosorbent) before and after adsorption (in single and ternary solution).

Peak near 3400 cm^{-1} was shifted to 3465 cm^{-1}, 3467 cm^{-1}, 3474 cm^{-1} for respective metals (Cd^{2+}, Ni^{2+} and Cr^{6+}) indicating the involvement of amino and hydroxyl groups. In the case of Ni^{2+} and Cr^{6+} an overlapping peak was generated at 3415 cm^{-1}. Two new peaks were generated at 480 cm^{-1} and 481 cm^{-1} in Cr^{6+} and Ni^{2+} adsorbed biomass may be the result of the complexation/coordination reaction during adsorption. Peak near 1400 cm^{-1} was slightly shifted to 1408 cm^{-1} for Cd^{2+}, 1381 cm^{-1}, and 1384 cm^{-1} for Ni^{2+} and Cr^{6+} respectively suggesting the participation of the phosphate group. Overall, metal sequestration critically changed biomass appearance.

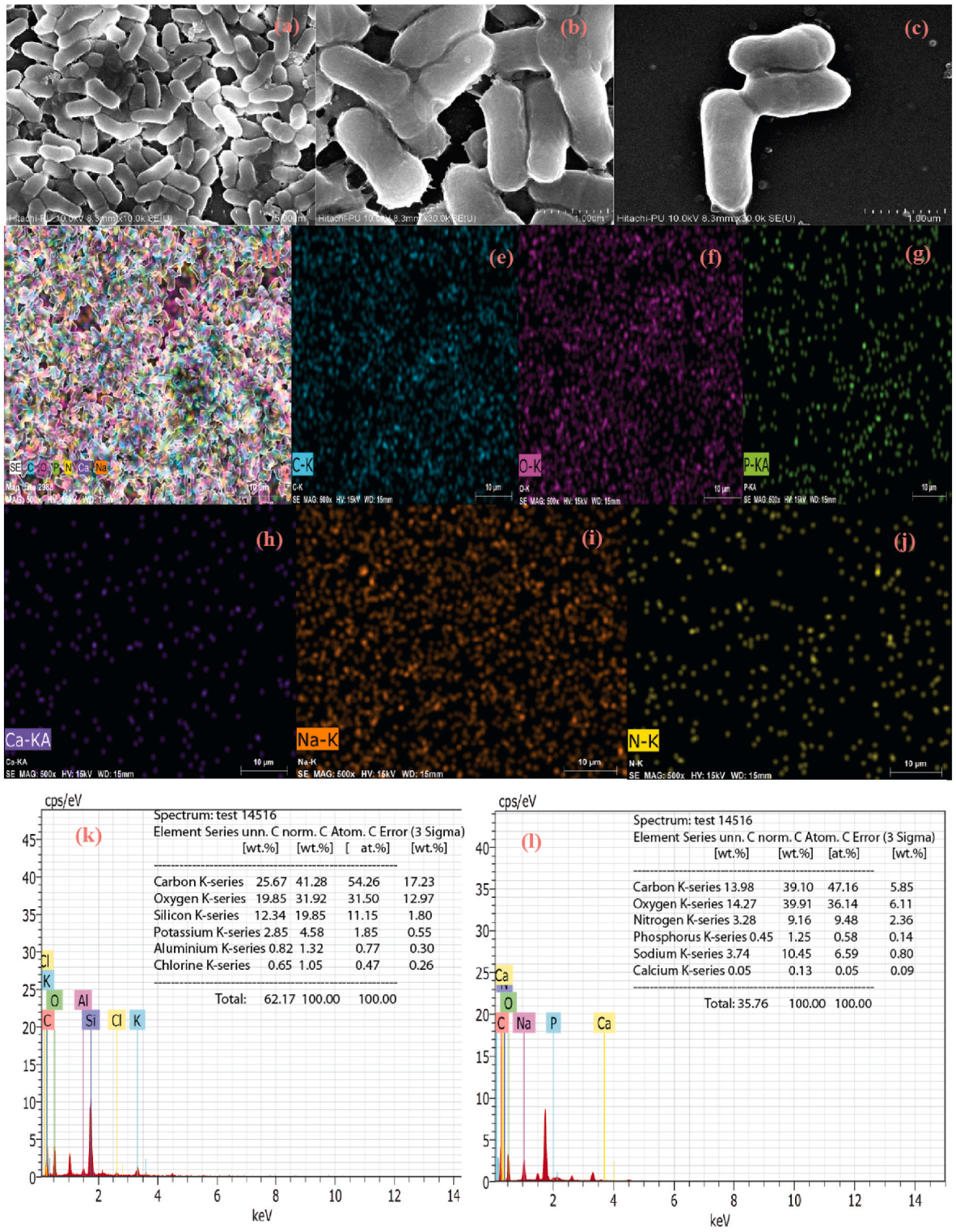

Fig. 5. (a–l) FESEM-EDAX image of *B. xiamenensis* ISIGRM16 (biosorbent) before metal biosorption.

3.8. Probable biosorption mechanism

The results confirmed the biosorption of Cd^{2+}, $Ni^{2+,}$ and Cr^{6+} by *Bacillus xiamenensis* ISIGRM16. It exhibited metabolically independent monolayered biosorption for Ni^{2+} and Cr^{6+} while multi-layered biosorption for Cd^{2+}. In this process the metal ions physically adsorbed onto the biomass surface via carboxyl, phosphate, hydroxyl, and amide groups (Fig. 7), which corresponds with the findings of Özdemir et al. (2009); Mathivanan et al. (2021) who studied surface active groups of *Bacillus* sp. responsible for adsorption. In general, physical adsorption is a faster process and reversible owing to Vander Wall forces and electrostatic interaction. Additionally, the bacterial cell surface is profusely composed of lipids, polysaccharides, proteins, and functional groups like carboxyl, hydroxyl, phosphate, and amide which act as ligands for metal binding. The generation of Ca peak in metal-adsorbed cells is an indication of the release of Ca during metal adsorption, confirming the

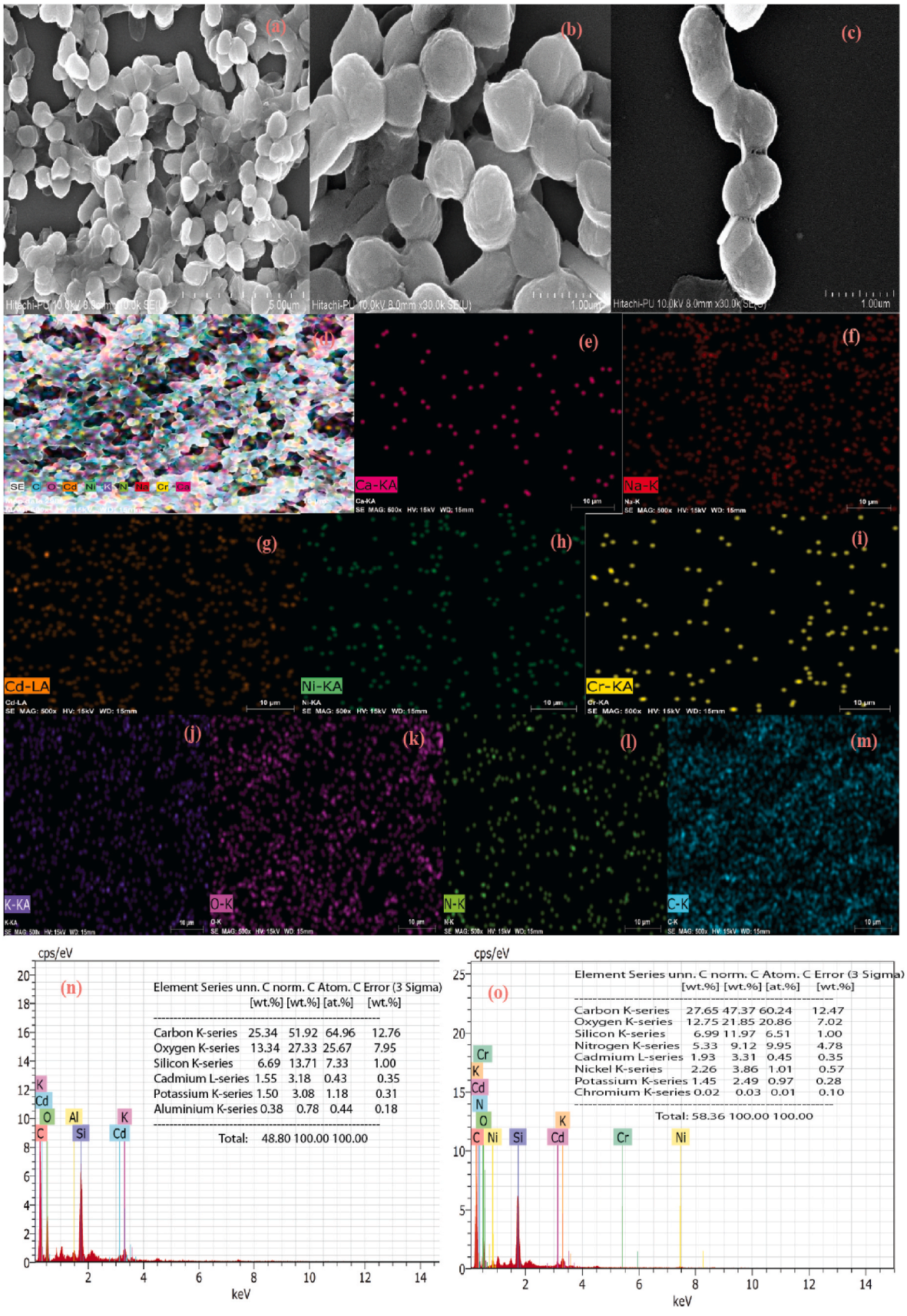

Fig. 6. (a–o) FESEM-EDAX image of *B. xiamenensis* ISIGRM16 (biosorbent) after metal biosorption.

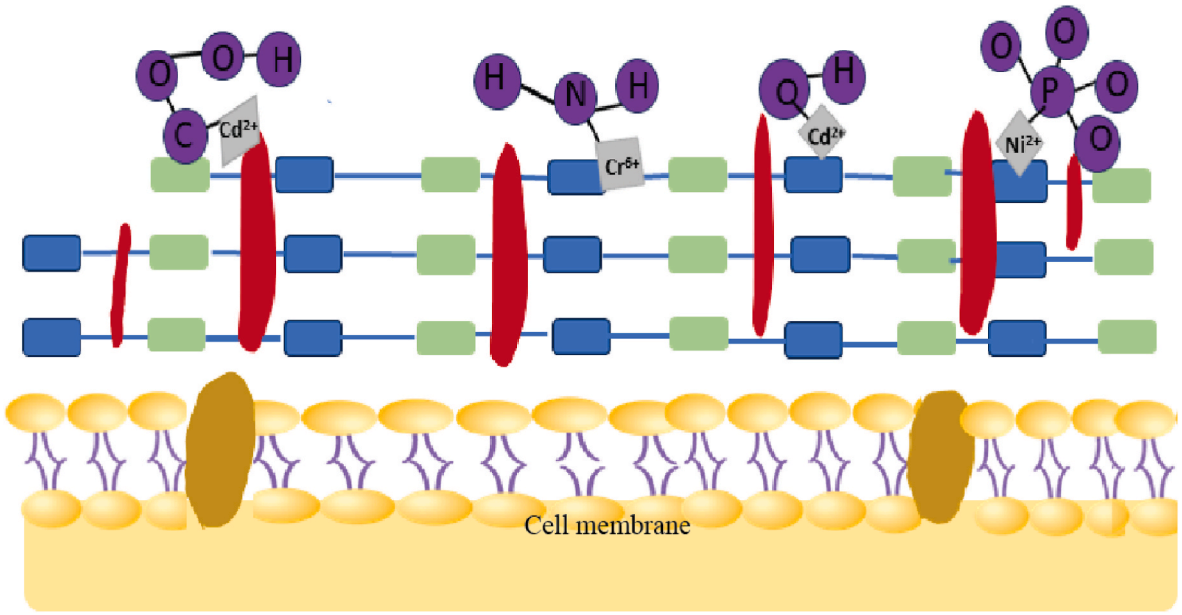

Fig. 7. A schematic diagram of metal biosorption on the cell surface of *B. xiamenensis* ISIGRM16.

occurrence of an ion exchange mechanism (Li et al., 2018). However, chelation and complexation coordination are different mechanisms bacteria opt for metal adsorption, thus, it is hard to conclude the exact mechanism of adsorption of the studied species.

3.9. Desorption and regeneration study

HCl was found to be the most efficient for Cd^{2+} with 98.76% ± 0.6 of recovery (Fig. 4c). HNO_3 showed the highest recovery rate for Ni^{2+} (97.73% ± 0.09) (Fig. 4c). While NaOH worked best for Cr^{6+} with the highest desorption ability of 72.07% ± 0.3 (Fig. 4c). The most efficient desorbent solution for each metal was used to complete the reusability investigation following Chatterjee et al. (2020), which involved five cycles of successive adsorption-desorption. After three cycles the adsorbent (biosorbent) showed a significant decrease in the removal of Cd^{2+} and Ni^{2+} (Fig. 4d) while for Cr^{6+} the removal capacity significantly decreased ($p < 0.05$) after second cycle (Fig. 4d). After fourth cycle and fifth cycle, the removal percent was decreased by 6% and 21% respectively for Cd^{2+} and Ni^{2+} was reduced by 17% and 21%. At the end of the fifth cycle, Cr^{6+} removal % drastically fell and decreased by 44.15%. It was evident that the biomass was able to remove metal ions up to 3rd cycle. After this, it reduced its uptake capacity ($p < 0.05$), however, for Cr^{6+} the biomass can successfully be utilized up to 2nd cycle. Thus, the reusability study indicated that the biomass of *Bacillus xiamenensis* ISIGRM16 can be reutilized for effective adsorption of metal ions.

3.10. Comparative assessment with contemporary biosorbent

The strain of the present study is compared with some previously identified bacterial, fungal, and algal biomass reported by different authors in terms of adsorption capacity by considering the parameters like pH and contact time for metal removal. The results are presented in a Table S4. The comparison fairly confirms that the studied bacterium has good adsorption capacity for all three metals (Cd^{2+}, Ni^{2+}, Cr^{6+}) when compared with these formerly studied strains. Hence, this novel *Bacillus xiamenensis* ISIGRM16 is proven to be a potent biosorbent for those precarious metallic species.

4. Conclusion

The study delivered a facile eco-friendly remedial approach using indigenous *Bacillus xiamenensis* ISIGRM16 which holds an excellent removal capacity of >99% Cd^{2+}, >85% Ni^{2+}, and >40% Cr^{6+}, making it a potent biosorbent. With a 3g L^{-1} dosage, the strain can remove about 99% Cd^{2+}, 85% Ni^{2+}, and 40% Cr^{6+} at pH 6 and 2; 30 °C and 45 °C, respectively. Apart from single-metal system, it performed well in multi-metal system and effectively removed Ni^{2+}> Cd^{2+}> Cr^{6+}. The Langmuir adsorption isotherm explained Ni^{2+} and Cr^{6+} biosorption whereas Cd^{2+} biosorption was best explained by the Freundlich isotherm model. The FESEM-EDS study verified the presence of metal deposition on the cell surface and the involvement of amide, carboxyl, phosphate, and hydroxyl in biosorption was confirmed using FTIR analysis. Desorption and regeneration study disclosed a high recovery rate of all metals (>98% Cd^{2+}, >97% Ni^{2+}, >70% Cr^{6+}) and effective removal potential up to 3rd cycle, making it a reusable and cost-effective biosorbent. Future research should include comprehensive environmental impact assessments to determine the ecological and long-term effects of using this technology in groundwater remediation, ensuring that it remains environmentally friendly throughout its lifecycle. Considering all these aspects, this environmentally-friendly bio-remedial approach can be easily scaled up for industrial applications, offering a promising and affordable purification technology. This opens new possibilities for inexpensive and sustainable water purification solutions.

CRediT authorship contribution statement

Kasturi Charan: Formal analysis, Investigation, Methodology, Writing - original draft, Data curation. **Jajati Mandal:** Software, Supervision, Visualization, Writing - review & editing, Conceptualization. **Pradip Bhattacharyya:** Conceptualization, Funding acquisition, Supervision, Writing - review & editing.

Declaration of competing interest

The authors declare that they have no known competing financial interests or personal relationships that could have appeared to influence the work reported in this paper.

Data availability

Data will be made available on request.

Appendix A. Supplementary data

Supplementary data to this article can be found online at https://doi.org/10.1016/j.gsd.2023.101063.

References

Adimalla, N., Sudarshan, V., 2018. Geochemical Characterization and Evaluation of Groundwater Suitability for Domestic and Agricultural Utility in Semi-arid Region of Basara, Telangana State, South India, 8. Applied Water Science.

Agnew, M.D., Koval, S.F., Jarrell, K.F., 1995. Isolation and characterization of novel alkaliphiles from bauxite-processing waste and description of Bacillus vedderi sp. nov., a new obligate alkaliphile. Syst. Appl. Microbiol. 18, 221–230.

Aksu, Z., Açikel, Ü., Kutsal, T., 1999. Investigation of simultaneous biosorption of copper (II) and chromium(VI) on dried *chlorella vulgaris*from binary metal mixtures: application of multicomponent adsorption isotherms. Separ. Sci. Technol. 34, 501–524.

Amin, M., Alazba, A.A., Shafiq, M., 2017. Nonspontaneous and multilayer adsorption of malachite green dye by *Acacia nilotica* waste with dominance of physisorption. Water Sci. Technol. 76, 1805–1815.

Chakraborty, J., Das, S., 2014. Characterization and cadmium-resistant gene expression of biofilm-forming marine bacterium *Pseudomonas aeruginosa* JP-11. Environ. Sci. Pollut. Control Ser. 21, 14188–14201.

Chakraborty, J., Mallick, S., Raj, R., Das, S., 2018. Functionalization of extracellular polymers of *Pseudomonas aeruginosa* N6P6 for synthesis of CdS nanoparticles and cadmium bioadsorption. J. Polym. Environ. 26, 3097–3108.

Chakraborty, V., Sengupta, S., Chaudhuri, P., Das, P., 2018. Assessment on removal efficiency of chromium by the isolated manglicolous fungi from Indian Sundarban mangrove forest: removal and optimization using response surface methodology. Environ. Technol. Innov. 10, 335–344.

Chakravarty, R., Banerjee, P., 2012. Mechanism of cadmium binding on the cell wall of an acidophilic bacterium. Bioresour. Technol. 108, 176–183.

Chang, J.S., Chen, C.C., 1998. Quantitative analysis and equilibrium models of selective adsorption in multimetal systems using a bacterial biosorbent. Separ. Sci. Technol. 33, 611–632.

Chatterjee, S., Mahanty, S., Das, P., Chaudhuri, P., Das, S., 2020. Biofabrication of iron oxide nanoparticles using manglicolous fungus Aspergillus niger BSC-1 and removal of Cr(VI) from aqueous solution. Chem. Eng. J. 385, 123790.

Chatterjee, S., Mahanty, S., Das, P., Chaudhuri, P., Das, S., 2022. Batch adsorption and process optimization for sequestration of Cr(VI) from aqueous solution using biofilm forming filamentous fungus *Aspergillus niger* BSC-1. J. Water Process Eng. 50, 103325.

Cherono, F., Mburu, N., Kakoi, B., 2021. Adsorption of lead, copper and zinc in a multi-metal aqueous solution by waste rubber tires for the design of single batch adsorber. Heliyon 7, e08254.

Congeevaram, S., Dhanarani, S., Park, J., Dexilin, M., Thamaraiselvi, K., 2007. Biosorption of chromium and nickel by heavy metal resistant fungal and bacterial isolates. J. Hazard Mater. 146, 270–277.

Courtney, R., Xue, S., 2019. Rehabilitation of bauxite residue to support soil development and grassland establishment. J. Cent. S. Univ. 26, 353–360.

Das, S., Dash, H.R., Chakraborty, J., 2016. Genetic basis and importance of metal resistant genes in bacteria for bioremediation of contaminated environments with toxic metal pollutants. Appl. Microbiol. Biotechnol. 100, 2967–2984.

Dey, S., 2021. Microbial resources of alkaline bauxite residue and their possible exploitation in remediation and rehabilitation. Geomicrobiol. J. 39, 219–232.

Dey, S., Paul, A.K., 2021. Evaluation of physio-biochemical potentials of alkaliphilic bacterial diversity in bauxite processing residues of diverse restoration history. Environmental Sustainability 4, 155–169.

Dey, U., Chatterjee, S., Mondal, N.K., 2016. Isolation and characterization of arsenic-resistant bacteria and possible application in bioremediation. Biotechnology Reports 10, 1–7.

Dhaliwal, S., Singh, J., Taneja, P.K., Mandal, A., 2019. Remediation techniques for removal of heavy metals from the soil contaminated through different sources: a review. Environ. Sci. Pollut. Control Ser. 27, 1319–1333.

Di Carlo, E., Boullemant, A., Courtney, R., 2019. A field assessment of bauxite residue rehabilitation strategies. Sci. Total Environ. 663, 915–926.

Di Carlo, E., Boullemant, A., Poynton, H.C., Courtney, R., 2020. Exposure of earthworm (*Eisenia fetida*) to bauxite residue: implications for future rehabilitation programmes. Sci. Total Environ. 716, 137126.

Dong, X., Huang, W.C., Bian, Y., Feng, X., Ibrahim, S.A., Shi, D., Qiao, X., Liu, Y., 2019. Remediation and mechanisms of cadmium biosorption by a cadmium-binding protein from lentinula edodes. J. Agric. Food Chem. 67, 11373–11379.

Dubinin, M.M., Zaverina, E.D., Radushkevich, L.V., 1947. Sorption, and structure of activated carbons, I. Investigation of organic vapor adsorption. Zhurnal Fizicheskoi Khimii 21, 1351–1362.

Eldin, M., Aly, K., Khan, Z.A., Mekky, A.E.M., Saleh, T.S., Al-Bogami, A.S., 2016. Removal of methylene blue from synthetic aqueous solutions with novel phosphoric acid-doped pyrazole-g-poly(glycidyl methacrylate) particles: kinetic and equilibrium studies. Desalination Water Treat. 57, 27243–27258.

Febrianto, J., Kosasih, A.N., Sunarso, J., Ju, Y., Indraswati, N., Ismadji, S., 2009. Equilibrium and kinetic studies in adsorption of heavy metals using biosorbent: a summary of recent studies. J. Hazard Mater. 162, 616–645.

Giovanella, P., Vieira, G.a.L., Otero, I.V.R., Pellizzer, E.P., De Jesus Fontes, B., Sette, L.D., 2020. Metal and organic pollutants bioremediation by extremophile microorganisms. J. Hazard Mater. 382, 121024.

Grass, G., Fricke, B., Nies, D.H., 2005. Control of expression of a periplasmic nickel efflux pump by periplasmic nickel concentrations. Biometals 18, 437–448.

Gupta, S., Kumar, A., 2019. Removal of nickel (II) from aqueous solution by biosorption on *A. barbadensis* Miller waste leaves powder. Appl. Water Sci. 9.

Gupta, S., Sharma, S.K., Kumar, A., 2019. Biosorption of Ni(II) ions from aqueous solution using modified Aloe barbadensis Miller leaf powder. Water Sci. Eng. 12, 27–36.

Gustafsson, J.P., 2023. Visual MINTEQ Ver. 4.0 (4.05. KTH, Sweden. Retrieved from. https://vminteq.com/download/.

Hoseini, A.A., Kaboosi, H., Ahmady-Asbchin, S., Ghorbanalinezhad, E., Ghadikolaii, F.P., 2020. Binary Biosorption of Cadmium(II) and Nickel(II) onto *Planococcus* Sp. Isolated from Wastewater: Kinetics, Equilibrium and Thermodynamic Studies, 5. Biomedical Research and Clinical Practice.

Jain, M., Garg, V., Kadirvelu, K., Sillanpää, M., 2015. Adsorption of heavy metals from multi-metal aqueous solution by sunflower plant biomass-based carbons. Int. J. Environ. Sci. Technol. 13, 493–500.

Jaishankar, M., Tseten, T., Anbalagan, N., Mathew, B.B., Beeregowda, K.N., 2014. Toxicity, mechanism and health effects of some heavy metals. Interdiscipl. Toxicol. 7, 60–72.

Kamranifar, M., Moslehi, M., Nasseh, N., Ghadirian, M., Rahimi, S.M., 2019. Removal of hexavalent chromium from aqueous solutions using almond green hull adsorbent magnetized by Fe3O4: isotherm, kinetic and thermodynamic studies. Desalination Water Treat. 165, 203–211.

Karunanidhi, D., Aravinthasamy, P., Subramani, T., Chandrajith, R., Raju, N.J., Antunes, I., 2022. Provincial and seasonal influences on heavy metals in the Noyyal River of South India and their human health hazards. Environ. Res. 204, 111998.

Khan, M., Ijaz, M., Chotana, G.A., Murtaza, G., Malik, A., Shamim, S., 2021. *Bacillus altitudinis* MT422188: a potential agent for zinc bioremediation. Ann. Finance 26, 228–248.

Krishna, P., Ahn, Y., Reddy, M.V., 2014. Bacterial diversity of extremely alkaline bauxite residue site of alumina industrial plant using culturable bacteria and residue 16S rRNA gene clones. Extremophiles 18, 665–676.

Kumar, M., Singh, A.K., Sikandar, M., 2018. Study of sorption and desorption of Cd (II) from aqueous solution using isolated green algae *Chlorella vulgaris*. Appl. Water Sci. 8.

Li, X., Li, D., Yan, Z., Y, A., 2018. Adsorption of cadmium by live and dead biomass of plant growth-promoting rhizobacteria. RSC Adv. 8, 33523–33533.

Mahanty, S., Chatterjee, S., Ghosh, S., Tudu, P., Gaine, T., Bakshi, M., Das, S., Das, P., Bhattacharyya, S., Bandyopadhyay, S.K., Chaudhuri, P., 2020. Synergistic approach towards the sustainable management of heavy metals in wastewater using mycosynthesized iron oxide nanoparticles: biofabrication, adsorptive dynamics and chemometric modeling study. J. Water Process Eng. 37, 101426.

Majhi, K., Let, M., Halder, U., Bandopadhyay, R., 2022. Copper adsorption potentiality of *Bacillus stercoris* GKSM6 and *Pseudomonas alcaliphila* GKSM11 isolated from singhbhum copper mines. Geomicrobiol. J. 40, 193–202.

Majhi, K., Let, M., Halder, U., Chitikineni, A., Varshney, R.K., Bandopadhyay, R., 2023. Copper removal capability and genomic insight into the lifestyle of copper mine inhabiting *Micrococcus yunnanensis* GKSM13. Environ. Res. 223, 115431.

Manasi, Rajesh, V., Kumar, A., Rajesh, N., 2014. Biosorption of cadmium using a novel bacterium isolated from an electronic industry effluent. Chem. Eng. J. 235, 176–185.

Masoudi, R., Moghimi, H., Azin, E., Taheri, R.A., 2018. Adsorption of cadmium from aqueous solutions by novel Fe3O4- newly isolated *Actinomucor* sp. bio-nanoadsorbent: functional group study. Artif. Cells, Nanomed. Biotechnol. 46, 1092–1101.

Mathivanan, K., Chandirika, J.U., Mathimani, T., Rajendran, R., Annadurai, G., Yin, H., 2021. Production and functionality of exopolysaccharides in bacteria exposed to a toxic metal environment. Ecotoxicol. Environ. Saf. 208, 111567.

Mekonnen, E., Yitbarek, M., Soreta, T.R., 2015. Kinetic and thermodynamic studies of the adsorption of Cr(VI) onto some selected local adsorbents. S. Afr. J. Chem. 68.

Mishra, T., Singh, N., Singh, N., 2016. Restoration of red mud deposits by naturally growing vegetation. Int. J. Phytoremediation 19, 439–445.

Mohapatra, R., Parhi, P.K., Pandey, S.K., Bindhani, B.K., Thatoi, H., Panda, C.S., 2019. Active and passive biosorption of Pb(II)using live and dead biomass of marine bacterium *Bacillus xiamenensis* PbRPSD202: kinetics and isotherm studies. J. Environ. Manag. 247, 121–134.

Nuhoglu, Y., Malkoç, E., 2009. Thermodynamic and kinetic studies for environmentaly friendly Ni(II) biosorption using waste pomace of olive oil factory. Bioresour. Technol. 100, 2375–2380.

Oves, M., Khan, M.S., Zaidi, A., 2013. Biosorption of heavy metals by *Bacillus thuringiensis* strain OSM29 originating from industrial effluent contaminated north Indian soil. Saudi J. Biol. Sci. 20, 121–129.

Özdemir, S., Kılınç, E., Poli, A., Nicolaus, B., Güven, K., 2009. Biosorption of Cd, Cu, Ni, Mn and Zn from aqueous solutions by thermophilic bacteria, *Geobacillus toebii* sub.sp. decanicus and *Geobacillus thermoleovorans* sub.sp. stromboliensis: equilibrium, kinetic and thermodynamic studies. Chem. Eng. J. 152, 195–206.

Page, A.L., Miller, R.H., Keeney, D.R., 1982. Methods of Soil Analysis - Part 2. Soil Sci Soc Am, Madison.

Palanivel, T.M., Sivakumar, N., Al-Ansari, A., 2020. Bioremediation of copper by active cells of *Pseudomonas stutzeri* LA3 isolated from an abandoned copper mine soil. J. Environ. Manag. 253, 109706.

Priyadarshanee, M., Das, S., 2021. Bioremediation potential of biofilm forming multi-metal resistant marine bacterium Pseudomonas chengduensis PPSS-4 isolated from contaminated site of Paradip Port, Odisha. J. Earth Syst. Sci. 130 (3), 125.

Quintelas, C., Rocha, Z., Silva, B., Fonseca, B., Figueiredo, H., Tavares, T., 2009. Removal of Cd(II), Cr(VI), Fe(III) and Ni(II) from aqueous solutions by an *E. coli* biofilm supported on kaolin. Chem. Eng. J. 149, 319–324.

Roy, R., Samanta, S., Pandit, S., Naaz, T., Banerjee, S., Rawat, J., Chaubey, K.K., Saha, R. P., 2023. An overview of bacteria-mediated heavy metal bioremediation strategies. Appl. Biochem. Biotechnol. https://doi.org/10.1007/s12010-023-04614-7.

Sağ, Y., Kutsal, T., 1996. Fully competitive biosorption of chromium (VI) and iron(III) ions from binary metal mixtures by *R. arrhizus*: use of the competitive Langmuir model. Process Biochem. 3, 573–585.

Sambrook, J., 2001. Molecular Cloning: A Laboratory Manual, Third Edition. Cold Spring Harbor Laboratory Press. (3 volume set) (3rd ed.).

Saravanane, R., Sundararajan, T., Sivamurthyreddy, S., 2002. Efficiency of chemically modified low cost adsorbents for the removal of heavy metals from wastewater: a comparative study. Indian Journal of Environmental Health 44, 78–81.

Shylla, L., Barik, S.K., Joshi, S.R., 2021. Characterization and bioremediation potential of native heavy-metal tolerant bacteria isolated from rat-hole coal mine environment. Arch. Microbiol. 203, 2379–2392.

Skodras, G., Diamantopoulou, I., Pantoleontos, G., Sakellaropoulos, G., 2008. Kinetic studies of elemental mercury adsorption in activated carbon fixed bed reactor. J. Hazard Mater. 158, 1–13.

Tuomikoski, S., Runtti, H., Romar, H., Lassi, U., Kangas, T., 2021. Multiple heavy metal removal simultaneously by a biomass-based porous carbon. Water Environ. Res. 93, 1303–1314.

United Nations Development Programme, 2006. Annual Report 2006–Global Partnership for Development, 27. United Nations Development Programme, New York. https://www.undp.org/sites/g/files/zskgke326/files/publications/UNDP-in-action-2006-en.pdf.

Verma, D.K., Hasan, S.H., Singh, D.K., Singh, S., Singh, Y., 2014. Enhanced biosorptive remediation of hexavalent chromium using chemotailored biomass of a novel soil isolate *Bacillus aryabhattai* ITBHU02: process variables optimization through artificial neural network linked genetic algorithm. Ind. Eng. Chem. Res. 53, 3669–3681.

Wen, L., Chen, Y., Wang, T., 2021. Cadmium biosorption by lactic acid bacteria *Weissella viridescens* ZY-6. Food Control 123, 107747.

Wiercigroch, E., Szafraniec, E., Czamara, K., Pacia, M.Z., Majzner, K., Kochan, K., Kaczor, A., Baranska, M., Malek, K., 2017. Raman and infrared spectroscopy of carbohydrates: a review. Spectrochim. Acta Mol. Biomol. Spectrosc. 185, 317–335.

Yahaghi, Z., Shirvani, M., Nourbakhsh, F., De La Peña, T.C., Pueyo, J.J., Talebi, M., 2018. Isolation and characterization of Pb-solubilizing bacteria and their effects on Pb uptake by *Brassica juncea*: implications for microbe-assisted phytoremediation. J. Microbiol. Biotechnol. 28, 1156–1167.